Research Paper

THEMED ISSUE: Subduction Top to Bottom 2

GEOSPHERE

GEOSPHERE, v. 17, no. 3

https://doi.org/10.1130/GES02338.1

12 figures; 1 table; 1 set of supplemental files

CORRESPONDENCE:
carmenrdealmodovar@gmail.com

CITATION: Castro, A., Rodriguez, C., Fernández, C., Aragón, E., Pereira, M.F., and Molina, J.F., 2021, Secular variations of magma source compositions in the North Patagonian batholith from the Jurassic to Tertiary: Was mélange melting involved?: Geosphere, v. 17, no. 3, p. 766–785, https://doi.org/10.1130/GES02338.1.

Science Editor: Shanaka de Silva
Guest Associate Editor: Robert J. Stern

Received 20 August 2020
Revision received 18 November 2020
Accepted 3 February 2021

Published online 21 April 2021

Secular variations of magma source compositions in the North Patagonian batholith from the Jurassic to Tertiary: Was mélange melting involved?

Antonio Castro[1], Carmen Rodriguez[2], Carlos Fernández[3], Eugenio Aragón[4], Manuel Francisco Pereira[5], and José Francisco Molina[6]

[1]Instituto Andaluz de Ciencias de la Tierra (IACT), Consejo Superior de Investigaciones Científicas–Universidad de Granada (CSIC-UGR), 18100 Armilla, Granada, Spain
[2]Geosciences Barcelona (formerly ICTJA), Consejo Superior de Investigaciones Científicas (CSIC), 08028 Barcelona, Spain
[3]Departamento de Ciencias de la Tierra, Universidad de Huelva, 21007 Huelva, Spain
[4]Facultad de Ciencias Naturales y Museo, Universidad Nacional de la Plata, B1900 La Plata, Buenos Aires, Argentina
[5]Instituto de Ciências da Terra (ICT), Departamento de Geociências, Escola de Ciências e Tecnologia (ECT), Universidade de Évora, 7000-670 Évora, Portugal
[6]Departamento de Mineralogía y Petrología, Universidad de Granada, Campus Univeristario de Fuentenueva, 18071 Granada, Spain

ABSTRACT

This study of Sr-Nd initial isotopic ratios of plutons from the North Patagonian batholith (Argentina and Chile) revealed that a secular evolution spanning 180 m.y., from the Jurassic to Neogene, can be established in terms of magma sources, which in turn are correlated with changes in the tectonic regime. The provenance and composition of end-member components in the source of magmas are represented by the Sr-Nd initial isotopic ratios ($^{87}Sr/^{86}Sr$ and $^{143}Nd/^{144}Nd$) of the plutonic rocks. Our results support the interpretation that source composition was determined by incorporation of varied crustal materials and trench sediments via subduction erosion and sediment subduction into a subduction channel mélange. Subsequent melting of subducted mélanges at mantle depths and eventual reaction with the ultramafic mantle are proposed as the main causes of batholith magma generation, which was favored during periods of fast convergence and high obliquity between the involved plates. We propose that a parental diorite (= andesite) precursor arrived at the lower arc crust, where it underwent fractionation to yield the silicic melts (granodiorites and granites) that formed the batholiths. The diorite precursor could have been in turn fractionated from a more mafic melt of basaltic andesite composition, which was formed within the mantle by complete reaction of the bulk mélanges and the peridotite. Our proposal follows model predictions on the formation of mélange diapirs that carry fertile subducted materials into hot regions of the suprasubduction mantle wedge, where mafic parental magmas of batholiths originate. This model not only accounts for the secular geochemical variations of Andean batholiths, but it also avoids a fundamental paradox of the classical basalt model: the absence of ultramafic cumulates in the lower arc crust and in the continental crust in general.

INTRODUCTION

Andean (= Cordilleran)–type batholiths represent large volumes of silicic ($SiO_2 > 53$ wt%) magmas that are generated at active continental margins. The subduction of lithosphere is, directly or indirectly, the triggering process for magma generation. However, fundamental issues like the source of magmas and the locus of melting, mantle or crust, still remain debated. Competing processes have been proposed, such as (1) the melting of a metasomatized mantle wedge by action of fluids from a downgoing slab (Grove et al., 2002, 2005; Kushiro, 1974) (2) assimilation and melting of continental crustal rocks triggered by invasion of basalts at the lower crust (Hildreth and Moorbath, 1988), and, more recently, (3) melting of subducted mélanges within the mantle wedge (Castro et al., 2010; Codillo et al., 2018; Cruz-Uribe et al., 2018). In principle, the three mechanisms may result in the generation of silicic melts and/or their intermediate parental magmas, leading finally to the formation of batholiths. However, requirements imposed by geochemical and isotopic ratios are better accounted for by mechanisms involving mixing of sources that occurred previous to melting within the mantle (Nielsen and Marschall, 2017) rather than mixing of melts from different sources or assimilation of crustal contaminants by mantle-derived basaltic melts (Davidson et al., 1991; Hildreth and Moorbath, 1988). Consequently, determining whether isotopic features are inherited from the source or acquired by magmas during their ascent and emplacement is an essential step to decipher the role of isotopic ratios in supporting or rejecting the aforementioned mechanisms. We show here new U-Pb sensitive high-resolution ion microprobe (SHRIMP) zircon ages and Sr-Nd isotopic data from plutons of the North Patagonian batholith (Chile and Argentina), which can unravel the secular geochemical evolution of magma source compositions from the Jurassic onwards. In subduction zones, this evolution is expected to entail changes in the relative contributions of geochemically evolved continental reservoirs (e.g., sediments and ancient continental crust) and altered oceanic crust. Although there is agreement about the presence of these end members in the composition of Andean (= Cordilleran) batholiths (DePaolo, 1981b; Hervé et al., 2007; Lee et al., 2006; Pankhurst et al., 1999), the mechanisms by which they are incorporated into magmas remain poorly constrained. We discuss the determination of these mechanisms through study of geochemical secular variations in plutons of the North Patagonian batholith.

It has been demonstrated, on the basis of partitioning of Sr and Nd between subducted rocks and fluids (Nielsen and Marschall, 2017), that metasomatism by fluids and/or melts derived from the subducted slab (the classical model) is unable to account for the observed geochemical and isotopic features of arc magmas. Alternatively, the direct participation of the whole subducted mélange, and not only fluids or melts from it, accounts for observed geochemical features. The participation of the mélange as a whole in the generation of arc magmas may be accomplished in two ways: (1) melting of mélange materials (closed system) at the core of silicic diapirs, as predicted by thermomechanical models (Gerya and Yuen, 2003; Gerya et al., 2004), and (2) reaction and complete digestion of the partially molten mélange, forming narrow channels within the surrounding peridotite (Kelemen, 1995; Kelemen et al., 2003). The two mechanisms have been experimentally tested for fertility and melt compositions. Experimental results matched the geochemical features of batholiths and arc magmas in general (Castro et al., 2010). Those results are central to the new paradigm of arc magma generation, which is referred to as the mélange diapir model (Marschall and Schumacher, 2012). In the first case, more than 50% of granodiorite melt—the most abundant rock type in Andean-type batholiths—is formed in equilibrium with plagioclase and pyroxene at 1100 °C and 1.5 GPa, and with garnet at 2.0 GPa (Castro et al., 2010, 2013). At temperatures >1100 °C, the melt composition tends to be dioritic, approaching the composition of the whole mélange system. In the second case, experiments using a homogeneous mixture of the KLB-1 lherzolite and mélange composed of a mid-ocean-ridge basalt (MORB)–amphibolite and Bt-rich gneiss at 1050–1300 °C and 1.0–1.5 GPa (Castro et al., 2013) yielded mafic melts matching the composition of andesites and basaltic andesites. Those mafic magmas will have hybrid geochemical signatures and can be the precursors of parental diorites and batholiths by fractionation within upper mantle and crust.

The selection of the North Patagonian batholith for this study was based on several grounds: (1) the protracted magmatic activity for ~180 m.y., from the Jurassic to Tertiary, (2) the changes marked in various tectonic regimes with time, and (3) the accessibility and previous knowledge of regional geology. Based on these particular conditions, we carried out a study of plutons across two traverses, aiming to correlate secular geochemical changes with variations in the tectonic regime of plate convergence and subduction.

GEOLOGICAL SETTING

The North Patagonian batholith is mostly composed of calc-alkaline granitic and intermediate rocks (diorites, quartz-diorites, tonalites, granodiorites, and monzogranites) that extend for ~800 km, from latitude 39°S to 46°S, along the western continental margin of South America. The North Patagonian batholith forms the core of the Southern Andes, a subduction orogenic belt active since the Middle Jurassic to present day. The study area includes the subduction of the Nazca plate beneath South America (Fig. 1C). The main geomorphological units present at this latitude are, from west to east: the Coastal Cordillera, Central Valley, Patagonian Andes, and extra-Andean Patagonia. The geology of this region is dominated by Late Jurassic, Cretaceous, and Neogene granitoids of the North Patagonian batholith (Aragón et al., 2011; Castro et al., 2011; Hervé et al., 2007; Pankhurst et al., 1999; Suárez and De La Cruz, 2001), and Cretaceous volcanic rocks (Fig. 1B). In the forearc, the morphological units are the southward continuation of the Coastal Cordillera and the Central Valley. The basement in the area is represented by a late Paleozoic–Triassic accretionary prism (Duhart et al., 2001; Forsythe, 1982; Hervé et al., 2008; Thomson and Hervé, 2002; Willner et al., 2000). The Coastal Cordillera shows the westward outcrops of Eocene plutons of the North Patagonian batholith.

The tectonic history of the studied region shows two periods of alternating extension-contraction: It started with extension and crustal thinning from the Late Jurassic to the Early Cretaceous, followed by contraction during mid-Cretaceous time. New extension and crustal thinning took place from the Late Cretaceous to late Oligocene, followed by contraction in the Neogene. The mid-Cretaceous deformational event was coeval with the mid-Cretaceous peak of magmatic input to the North Patagonian batholith.

SAMPLING AND ANALYTICAL TECHNIQUES

Sampling for this study was carried out in two campaigns in 2011 and 2015, mostly concentrated in the area of Aysén (Chile), where a Mesozoic–Tertiary paired belt of plutons extends parallel to the present-day trench and represents the Mesozoic (mostly Cretaceous) plutons dominating in volume in the inner belt. Also, dated samples from the area of Bariloche to the north of Aysén (Castro et al., 2011) were analyzed for Sr and Nd isotopes for this study. In total, 40 representative samples, collected across the two traverses of the North Patagonian batholith in Aysén (Chile) and Bariloche (Argentina) (Figs. 1A and 1B), were analyzed to determine whole-rock geochemistry (major and trace elements) and isotopic ratios (Sr and Nd). A selection of samples from the Aysén area was analyzed by in situ SHRIMP U-Pb age determination. Petrographic studies and microprobe analyses of relevant mineral phases (amphibole, pyroxene, and plagioclase) were also carried out on the dated samples, with particular attention to amphibole chemistry in order to determine pressure and temperature conditions of crystallization. Thin sections of intrusive rocks were polished and subsequently analyzed. Microprobe analyses were carried out by wavelength-dispersive (WD) spectrometry with a JEOL JXA-8200 Superprobe at the University of Huelva, Huelva, Spain. A combination of silicates and oxides was used for calibration, and a 5-µm-diameter beam was selected to reduce the Na migration.

Approximately 500 g aliquots of each sample were ground for whole-rock geochemical analysis. Major elements and Zr were determined by X-ray fluorescence (XRF) at the Centro de Instrumentación Científica, University of Granada, Granada, Spain. Trace elements, including rare earth elements (REEs), were determined by inductively coupled plasma–mass spectrometry (ICP-MS), also at the University of Granada, following standard procedures

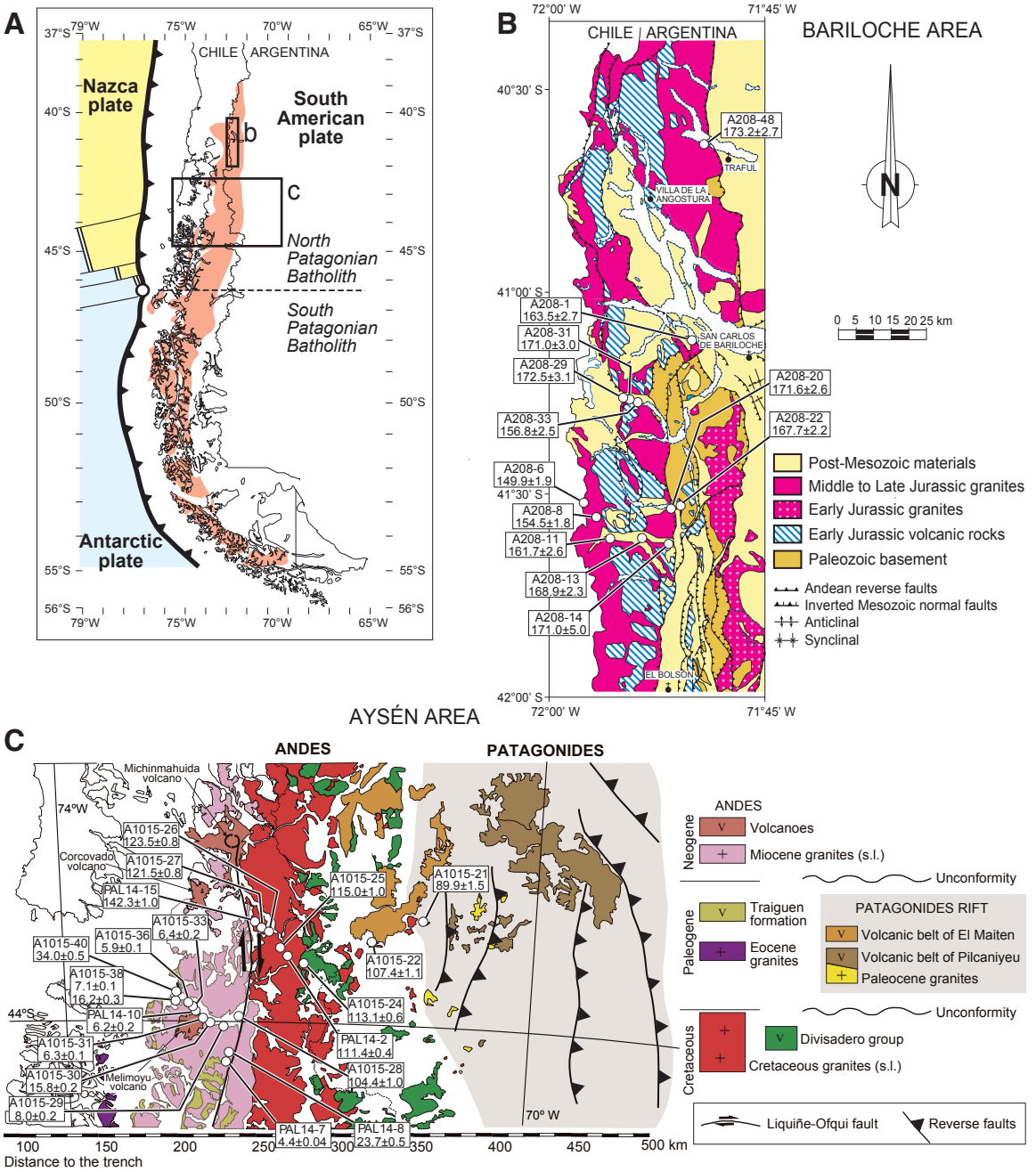

Figure 1. (A) Tectonic environment of the North Patagonian batholith in South America. (B–C) Geology and sample locations in the studied traverses of Bariloche (B) and Aysén (C). U-Pb zircon ages are labeled. Geological schematic maps of B and C are after published maps from the Geological Surveys of Argentina and Chile (downloaded from the Servicio Geológico Minero Argentino, SEGEMAR, Digital Cartography, https://sigam.segemar.gov.ar/, and the Servicio Nacional de Geología y Minería, Chile, SERNAGEOMIN, Geological Map of Chile, digital version, http://www.ipgp.fr/~dechabal/Geol-millon.pdf).

(Baedecker, 1987). Precision for major elements was better than 1% relative. Analyses of trace elements were performed following the method described in Bea (1996); the precision was ~2% and 5% error on concentrations of 50 and 5 ppm, respectively. Samples for Sr and Nd isotope analyses were digested in a clean room using ultraclean reagents and analyzed by thermal ionization mass spectrometry (TIMS) in a Finnigan Mat 262 spectrometer after chromatographic separation with ion-exchange resins. Normalization values were $^{86}Sr/^{88}Sr$ = 0.1194 and $^{146}Nd/^{144}Nd$ = 0.7219. Isotopic ratios of $^{87}Rb/^{86}Sr$ and $^{147}Sm/^{144}Nd$ were directly determined by ICP-MS (Montero and Bea, 1998) with a precision, estimated by analyzing 10 replicates of the standard WS-E, better than 1.2% and 0.9% (2σ), respectively.

Traditional techniques using dense liquids, magnetic separation, and handpicking were performed for zircon separation. Zircon crystals of distinct morphology and size were separated from each sample of igneous rock and cast on epoxy mounts that also included three zircon standards used for calibration procedures. TEMORA (ca. 417 Ma) was used as isotope ratio standard zircon (Black et al., 2003), SL13 was used as concentration standard (238 p.m. U) (Claoue-Long et al., 1995) and GAL (ca. 480 Ma) was used for very high U, Th, and common Pb content (Montero and Bea, 1998). Before selection of targets, the internal morphology of the zircon crystals was analyzed using cathodoluminescence (CL) images previously obtained through a CL detector coupled to a scanning electron microscope (SEM). Then, selected zircon crystals were analyzed for U-Th-Pb geochronology using SHRIMP at the IBERSIMS laboratory (University of Granada). Targets were rastered by a primary beam for 120 s prior to analysis. Then, the selected area was analyzed over six scans by running the peak sequence: $^{196}Zr_2O$, ^{204}Pb, $^{204.1}$background, ^{206}Pb, ^{207}Pb, ^{208}Pb, ^{238}U, ^{248}ThO, and ^{254}UO. Every peak of each scan was measured sequentially 10 times according to the total counts per scan: 2 s for mass 196; 5 s for masses 238, 248, and 254; 15 s for masses 204, 206, and 208; and 20 s for mass 207. The incidence of the primary beam, with an intensity of 4–5 nA and using a 120 µm Kohler aperture, on the target produced an elliptical crater (17 × 20 µm). A resolution of ~5000 AMU (atomic mass units) at 1% peak height was reached by the secondary beam exit slit set at 80 µm. Mass calibration was performed on the GAL zircon, analytical sessions initially involved the measurement of the SL13 zircon, and TEMORA zircon was used as the isotope ratio standard, measured every four unknowns. A more detailed description of the analytical procedures and data reduction can be seen at the site: https://www.ugr.es/~ibersims/ibersims/Methods.html. U-Pb data were processed with ISOPLOT software (Ludwig, 2003) for concordia diagrams and weighted average and concordia age calculations.

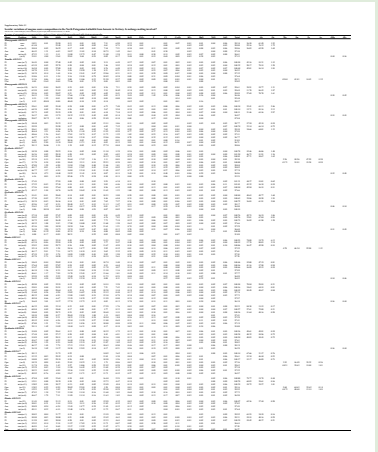

[1]Supplemental Material. Geochemical and geochronologic data. Please visit https://doi.org/10.1130/GEOS.S.13705915 to access the supplemental material, and contact editing@geosociety.org with any questions.

RESULTS

Mineral and Petrographic Features

Plutons of the North Patagonian batholith are composed of homogeneous diorites, tonalites, granodiorites, and monzogranites. Textural variations are marked by grain size and color index, which usually show transitions. Magmatic layered structures are common near the contacts, where accumulation of mafic minerals and segregation of felsic layers are observed (Figs. 2A and 2B). Mingling zones with dark pillows included into felsic granites are common structures, indicating magma behavior during the magma emplacement and recharge of subvolcanic magma chambers. Xenoliths from older granitic intrusions are also common (Figs. 2C and 2D). Some plutons show subvolcanic porphyritic textures with a fine-grained matrix and abundant plagioclase phenocrysts. Diorites and quartz-diorites are composed of Pl, Opx, Cpx, Amp, Ox ± Qz, ± Bt (mineral abbreviations after Whitney and Evans, 2010). Tonalites, granodiorites, and monzogranites are mostly composed of Pl, Bt, Kfs, Qz, Amp, ± Cpx (Table S1[1]). Plagioclase shows the typical complex oscillatory zoning that characterizes calc-alkaline granitic rocks. The composition ranges from An_{51} (subscript denotes mole %) in diorites and quartz-diorites to An_{32} in granodiorites and monzogranites. Clinopyroxene of diorites and quartz-diorites has the composition $Wo_{44}En_{39}Fs_{16}$, whereas orthopyroxene is $Wo_{03}En_{54}Fs_{35}$ (Table S1). Amphibole compositions range from 6.3 to 7.2 apfu (atoms per formula unit) of Si and 0.4–0.8 in the Mg/(Mg + Fe) ratio. Most of them are classified as Mg-hornblende, with a very few classified as tschermakitic hornblende and actinolite. Biotite is systematically present in most samples, replacing amphibole and with euhedral and interstitial habit. A list of mineral compositions from each sample is given in the Supplemental Material (Table S1).

Figure 2 shows representative textures of diorites and granodiorites of the Aysén region. Descriptions of the Bariloche region were given in Castro et al. (2011). Amphibole is a late phase in the crystallization sequence. Euhedral faces are only observed in contact with Qz but not with Pl (Fig. 2E). Plagioclase forms large euhedral crystals, leaving Kfs and Qz in the interstices. Euhedral Amp may appear at these interstices together with Qz, denoting the late crystallization of a porous residual liquid (Fig. 2F). Resorbed An-rich cores are common (Fig. 2G), indicating repeated episodes of crystallization and dissolution. Clinopyroxene appears resorbed and replaced by Amp (Fig. 2H), indicating late rehydration of a residual liquid.

Whole-Rock Geochemical Features

According to bulk-rock geochemistry, plutonic rocks are separated in two groups: (1) a silica-rich (SiO_2 >63 wt%) granitic group ranging in composition from tonalites to granodiorites and granites, and (2) a basic to intermediate group (SiO_2 <63 wt%) formed by hornblende-biotite diorites and quartz-diorites. In the latter group, we included atypical low-silica rocks (SiO_2 <52 wt%) with MgO <8 wt% (many at ~6 wt% MgO), variable TiO_2, and K_2O <1 wt%. Most of these atypical diorites have Mg# within the range 0.5–0.6, where Mg# = molar MgO/(MgO + FeO^T), and T stands for total iron as FeO. Similar to other Andean-type batholiths (Castro, 2020), plutonic rocks of the North Patagonian batholith are magnesian, plotting below Miyashiro's line separating tholeiitic (ferroan) from calc-alkaline (magnesian) series on the basis of the

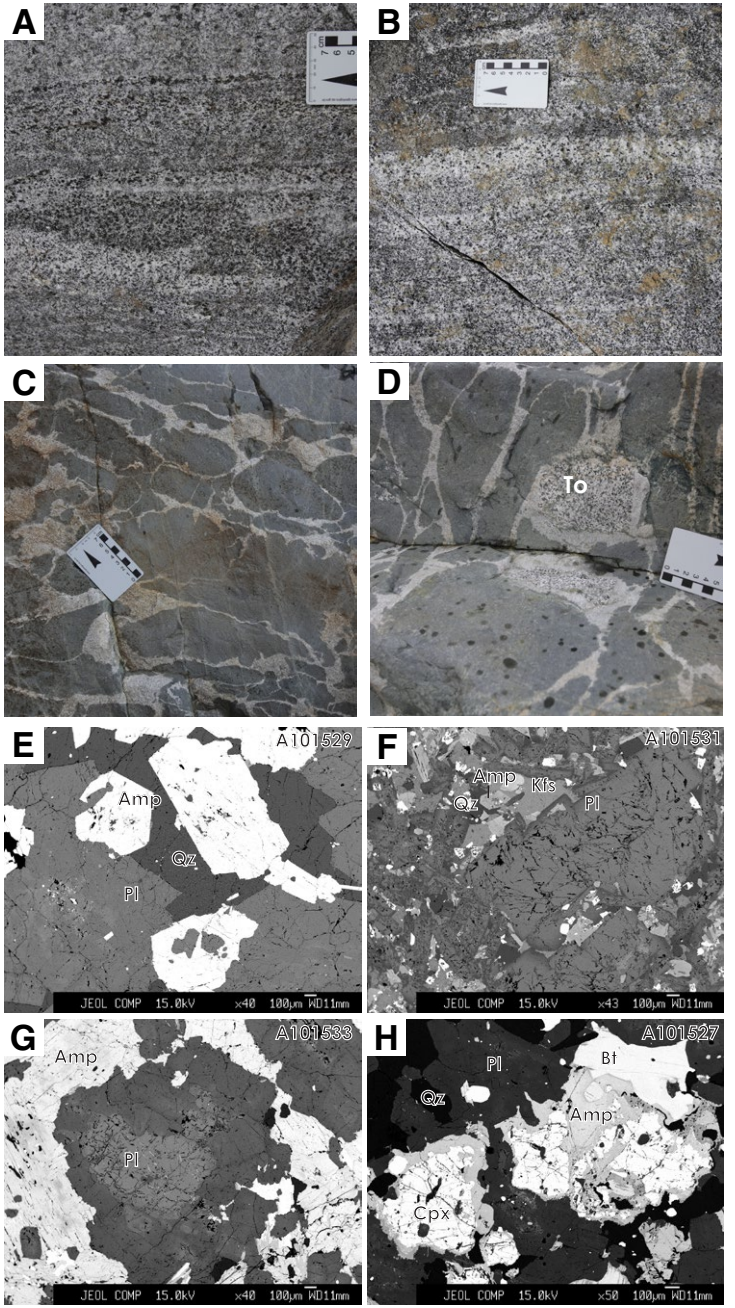

Figure 2. Representative structures and petrographic relations of rocks from the North Patagonian batholith in the Aysén region. (A, B) Magmatic layering with concentrations of mafic minerals (Bt and Amp) alternating with granitic layers (San Nicolás bridge). (C, D) Mingling relations of diorites (dark) and granites with inclusions of xenoliths from a tonalite (To) host (area between Melimoyu and Correntoso creeks, Chile). (E–H) Backscattered electron images (atomic number Z-contrast) showing representative relations of diorites and granodiorites of the Aysén region. Abbreviations of mineral names are after Whitney and Evans (2010). See text for details.

FeO/(FeO^T + MgO) ratio (Frost et al., 2001; Miyashiro, 1974), and calc-alkalic according to the alkali-lime Peacock index. They are metaluminous to weakly peraluminous at silica values of >70 wt% SiO_2 and show linear variations in Harker variation diagrams, which are compatible with magmatic differentiation (Fig. 3). Trace elements show depletion in Nb, compared with the neighbors K and La, in the MORB-normalized diagrams (Fig. 4A), and enrichment in large ion lithophile elements (LILEs), mostly following the pattern of continental andesites. Granites (SiO_2 >63 wt%), as the most fractionated rocks, show depletions in elements such as Sr, P, Zr, Hf, and Ti, which are partitioned to the coexisting solid assemblage. Differences in chondrite-normalized REEs between diorites and granites (Figs. 4B–4E) occur irrespective of the age of generation. Mesozoic and Tertiary diorites display gentle slope patterns with positive Eu anomalies in some samples and slightly negative or no anomaly in others. Granites display more fractionated patterns with higher light REE/heavy REE ratios. Those relations are compatible with fractionation of granites from diorites and, in both cases, in the absence of heavy REE fractionating phases such as garnet.

A complete list of isotopic ratios is given in Table 1. With the exception of two samples (PAL14–7 and PAL14–8), the rest of the dated samples were analyzed for Sr-Nd isotopes. Strontium isotopic initial ratios varied within a narrow range of $(^{87}Sr/^{86}Sr)_i = 0.7037–0.7065$. Neodymium initial ratios ($^{143}Nd/^{144}Nd$) were normalized to bulk earth ratios and are given in epsilon (ε) notation, ranging from −2.66 to +3.19 ε units. The most primitive ratios were displayed by the youngest plutons of the Aysén region. Isotopic mixing curves were calculated using the general mass balance equations for Sr and Nd (in mg/kg; ppm in the equations) and the respective initial isotopic ratios of end members involved:

$$\left(\frac{^{87}Sr}{^{86}Sr}\right)^{Mix} = \left[\left(\frac{^{87}Sr}{^{86}Sr}\right)^{B} \cdot Sr^{B}_{ppm} \cdot X_B\right] + \left[\left(\frac{^{87}Sr}{^{86}Sr}\right)^{CC} \cdot Sr^{CC}_{ppm} \cdot (1 - X_B)\right], \quad (1)$$

and

$$\left(\frac{^{143}Nd}{^{144}Nd}\right)^{Mix} = \left[\left(\frac{^{143}Nd}{^{144}Nd}\right)^{B} \cdot Nd^{B}_{ppm} \cdot X_B\right] + \left[\left(\frac{^{143}Nd}{^{144}Nd}\right)^{CC} \cdot Nd^{CC}_{ppm} \cdot (1 - X_B)\right], \quad (2)$$

where X_B refers to the fraction of oceanic crust in the mixture, and the superscripts *Mix*, *B,* and *CC* refer to the isotopic ratios of mixture, oceanic crust, and continental crust, respectively. For the end-member *B*, the average composition

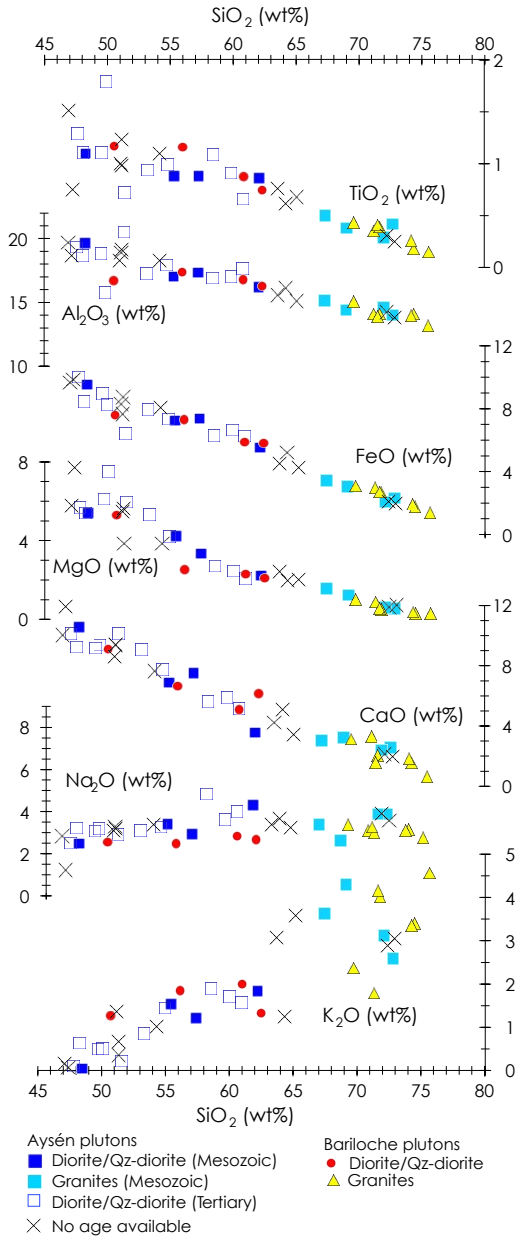

Figure 3. Silica variation diagrams (Harker) showing the trend of representative samples from the North Patagonian batholith in the regions of Aysén and Bariloche. Qz—quartz.

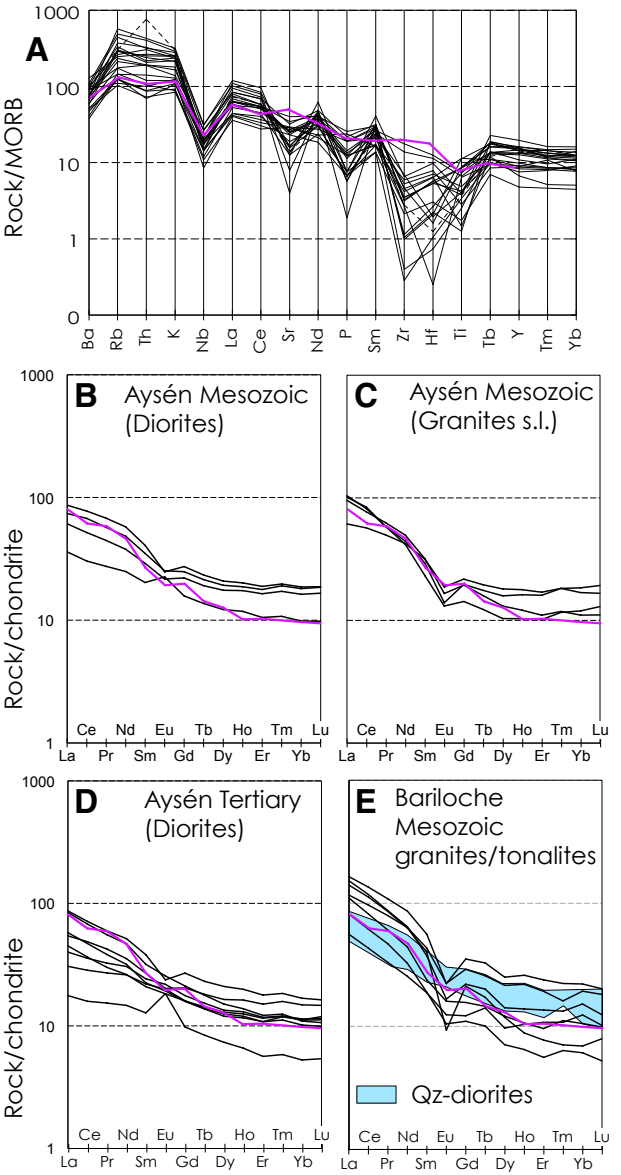

Figure 4. Trace-element diagrams of samples from the North Patagonian batholith. (A) Mid-ocean-ridge basalt (MORB)–normalized (Thompson et al., 1984) spider diagram. (B–E) Chondrite-normalized (Nakamura, 1974) plots of rare earth elements (REEs) comparing patterns of dioritic and granitic rocks from the Bariloche and Aysén regions. In all diagrams, the average composition of continental andesites (Kelemen et al., 2003) is shown (purple line). Qz—quartz.

TABLE 1. Sr AND Nd ISOTOPES OF SAMPLES FROM NORTH PATAGONIAN BATHOLITH

Sample	SiO_2 (wt%)	Age (Ma)	Rb (ppm)	Sr (ppm)	$^{87}Rb/^{86}Sr$	$^{87}Sr/^{86}Sr$	±2SD	$(^{87}Sr/^{86}Sr)i$	Sm (ppm)	Nd (ppm)	$^{147}Sm/^{144}Nd$	$^{143}Nd/^{144}Nd$	±2SD	$\varepsilon_{Nd}(t)$	T_{DM} (Ga)
A1015-36	54.33	5.9 ± 0.1	29.8	380.7	0.2267	0.70429	0.002	0.70429	4.067	16.54515	0.1486	0.512728	0.003	1.80	0.71
pal14-10	54.95	6.24 ± 0.1	42.9	305.2	0.4065	0.70424	0.002	0.70420	3.978	16.19671	0.1485	0.512784	0.002	2.89	0.57
A1015-31	48.25	6.4 ± 0.2	15.9	504.3	0.0915	0.70419	0.003	0.70418	3.593	13.96627	0.1555	0.512800	0.002	3.19	0.54
A1015-33	53.34	6.4 ± 0.2	23.4	303.5	0.2234	0.70423	0.003	0.70421	3.101	12.00641	0.1562	0.512658	0.003	0.42	0.76
A1015-29	60.01	8 ± 0.2	60.5	301.9	0.5803	0.70473	0.002	0.70466	5.652	23.60631	0.1448	0.512722	0.001	1.69	0.66
A1015-30	60.95	15.8 ± 0.2	43.9	337.9	0.3760	0.70402	0.003	0.70393	3.324	14.53171	0.1383	0.512756	0.003	2.42	0.61
A1015-38	51.54	15.9 ± 0.1 core: 16.1 ± 0.2	5.3	468.7	0.0326	0.70426	0.004	0.70425	5.458	5.45799	0.6046	0.512654	0.003	–0.52	0.84
A1015-40	47.80	33.9 ± 0.4	4.2	500.8	0.0243	0.70418	0.003	0.70417	1.893	6.72798	0.1702	0.512775	0.002	2.79	0.60
A1015-21	55.27	90 ± 1.4	31.2	502.1	0.1799	0.70447	0.002	0.70424	4.577	17.52201	0.1579	0.512729	0.002	2.22	0.68
A1015-28	55.46	104.4 ± 0.8	44.7	408.8	0.3166	0.70489	0.003	0.70442	6.023	26.35040	0.1382	0.512628	0.003	0.58	0.82
A1015-22	67.44	107 ± 1	130.4	291.9	1.2932	0.70630	0.003	0.70434	4.717	22.64045	0.1259	0.512641	0.002	1.02	0.79
A1015-24	72.83	113 ± 0.6	81.6	222.0	1.0631	0.70566	0.003	0.70395	4.672	19.40342	0.1456	0.512686	0.003	1.67	0.75
A1015-25	72.12	114.7 ± 1.6	104.1	183.6	1.6417	0.70637	0.004	0.70369	3.434	19.07199	0.1089	0.512703	0.004	2.56	0.68
A1015-27	57.41	121.7 ± 0.7	36.1	345.3	0.3028	0.70456	0.002	0.70404	4.296	17.29306	0.1502	0.512617	0.004	0.31	0.86
A1015-26	69.15	123.7 ± 0.5	105.9	164.4	1.8651	0.70754	0.003	0.70425	4.338	20.28848	0.1293	0.512698	0.002	2.24	0.71
pal14-15	48.46	142.8 ± 0.8	3.6	432.1	0.0238	0.70567	0.003	0.70562	3.002	11.40509	0.1591	0.512565	0.002	–0.74	0.96
A-208-6	71.32	149.9 ± 1.9*	38.7	273.9	0.4085	0.70592	0.003	0.70505	2.777	11.65600	0.1440	0.512690	0.002	2.02	0.75
A-208-8	50.71	154.5 ± 1.8*	51.0	341.2	0.4322	0.70577	0.003	0.70482	3.418	13.40100	0.1542	0.512608	0.002	0.25	0.89
A-208-33	74.50	156.8 ± 2.5*	116.2	149.7	2.2471	0.71020	0.003	0.70519	2.803	14.90100	0.1137	0.512527	0.003	–0.50	0.95
A-208-11	62.48	161.7 ± 2.6*	43.0	314.6	0.3953	0.70560	0.003	0.70469	5.907	24.91400	0.1433	0.512650	0.002	1.34	0.81
A-208-1	75.66	163.5 ± 2.7*	198.5	93.7	6.1404	0.71932	0.003	0.70504	5.909	28.71800	0.1244	0.512450	0.002	–2.16	1.09
A-208-22	69.74	166.7 ± 2.2*	61.2	294.1	0.6027	0.70725	0.003	0.70581	3.528	20.14400	0.1059	0.512403	0.002	–2.64	1.13
A-208-13	71.80	168.9 ± 2.3*	155.0	161.0	2.7874	0.71189	0.003	0.70519	6.396	29.07100	0.1330	0.512498	0.002	–1.36	1.03
A-208-14	60.98	171 ± 5*	74.1	378.3	0.5673	0.70720	0.003	0.70582	6.460	30.42300	0.1284	0.512425	0.002	–2.66	1.13
A-208-31	74.30	171 ± 3*	92.0	187.8	1.4174	0.70859	0.003	0.70514	5.553	29.50000	0.1138	0.512528	0.002	–0.34	0.95
A-208-20	71.64	171.6 ± 2.6*	170.2	145.8	3.3798	0.71304	0.003	0.70480	8.312	39.45300	0.1274	0.512438	0.002	–2.38	1.11
A-208-29	56.14	172.5 ± 3.1*	50.6	473.0	0.3093	0.70525	0.003	0.70449	6.123	25.49500	0.1452	0.512500	0.002	–1.56	1.05
A-208-48	77.55	173.2 ± 2.7*	86.3	47.0	5.3248	0.71959	0.003	0.70648	6.439	30.51400	0.1276	0.512547	0.002	–0.25	0.94

Note: SD—standard deviation; TDM—depleted mantle model.
*U-Pb zircon ages were taken from Castro et al. (2011).

of Sr-rich altered oceanic crust from Ocean Drilling Program (ODP) Site 801 was used (Kelley et al., 2003), and the isotopic initial ratios from the mean composition of ocean-ridge basalts were used (Gale et al., 2013). An analysis of secular variations of isotopic ratios is given in the Discussion.

Amphibole Thermobarometry

Amphibole was present in nearly all studied rocks in the Aysén and Bariloche regions. It was analyzed with an electron microprobe, together with associated plagioclase and occasionally pyroxene, in samples analyzed for zircon dating and isotopic relations. The aim was to obtain the temperature, pressure, and water content data of magmas at the time of crystallization. A complete list of amphibole analyses and calculations is given in the Supplemental Material (Table S4). Thermobarometric and hygrometric data were obtained with the equations of Ridolfi and Renzulli (2012) and are shown in pressure-temperature (*P*-*T*) and temperature-water (*T*-H_2O) diagrams (Fig. 5). Equation 1b of Ridolfi and Renzulli (2012) was used for pressure calculations. All samples were equilibrated at low pressure (300–100 MPa), and most of them below 200 MPa. With exception of a Tertiary diorite from Aysén (A1015–38) that yielded the highest temperature at ~900 °C, the rest of the samples clustered at 800 °C (840 °C at maximum).

Furthermore, *P*-*T* conditions of magma emplacement were also estimated with the new calibrations of the amphibole-plagioclase NaSi-CaAl exchange thermometer (Molina et al., 2020) using the expressions A1, A2, and B2 (precision ~±50 °C), and the Si/Al amphibole-plagioclase partitioning barometer from Molina et al. (2015) (Fig. 5; Table S5). Calculations were done with expressions A1 and A2 at 0.1 and 1.5 GPa, as these show a negligible pressure dependence,

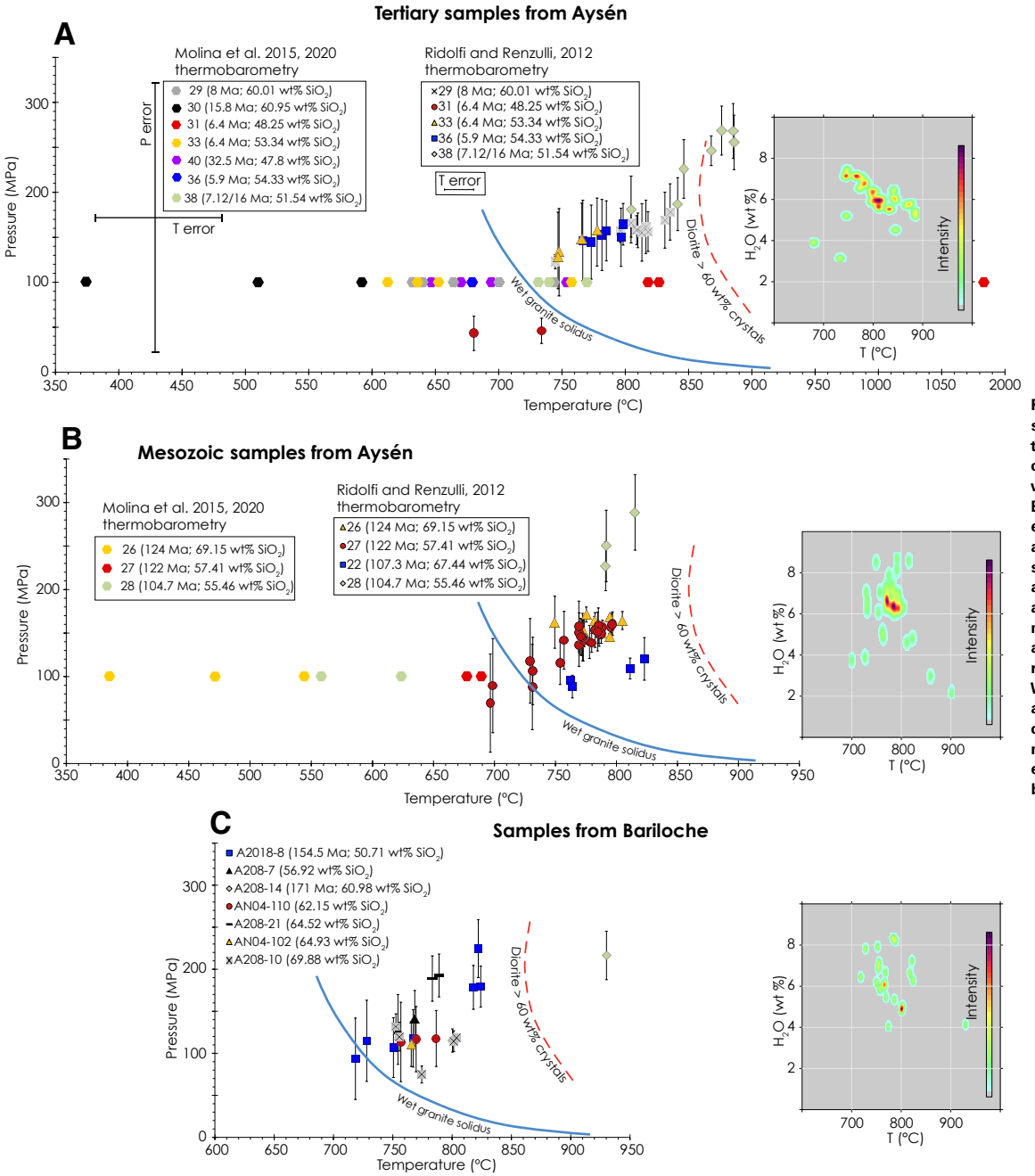

Figure 5. Pressure-temperature plots showing the results of amphibole thermobarometric and hygrometric calculations (Ridolfi and Renzulli, 2012) with samples from Aysén (A, B) and Bariloche (C). Pl-Amp-Pl thermobarometry results (Molina et al., 2015, 2020) are shown for Aysén samples for a constant pressure of 100 MPa, considered as a subvolcanic pressure. Error bars are displayed below the legend for each method. Amphibole hygrometric results are shown as Kernel density plots at the right of pressure-temperature diagrams. Wet granite solidus are after Johannes and Holtz (1996). The curve of 60 wt% crystals is traced by thermodynamic modeling with Rhyolite-MELTS (Gualda et al., 2012). Analyzed samples are labeled indicating the silica content.

and with expression B2, which is not pressure related (Molina et al., 2020). Average values of temperatures were used for the barometric calculations. Temperature estimates were even lower than those calculated by the equations of Ridolfi and Renzulli (2012). Temperatures for diorites, considering the three expressions together, are 724–761 °C at the cores of amphibole and plagioclase, decreasing to 642–703 °C at the rims. In quartz-diorites, temperature estimates are more homogeneous, ranging from 667 °C to 707 °C. Pressure estimates for both diorites and quartz-diorites cluster around zero, thus being consistent with magma crystallization in a shallow environment.

These temperatures were compared (Fig. 5) with the position of the water-saturated granite minimum (Johannes and Holtz, 1996) and the curve for 60 wt% crystals of diorite A1015–36 with 2 wt% initial water, calculated with the Rhyolite–MELTS thermodynamic model (Gualda et al., 2012). Melt water content in equilibrium with amphibole was estimated by amphibole hygrometry (Ridolfi and Renzulli, 2012).

U-Pb Zircon Geochronology

In total, 492 spots from 19 North Patagonian batholith plutonic rocks in the Aysén area were analyzed for U-Pb SHRIMP zircon geochronology. Zircon crystals showed a wide range in size and morphology, from rounded (subhedral) to prismatic (euhedral), including simple crystals, composite cores with simple concentric zoning, banded zoning, one or more overgrowths, and unzoned sectors. Descriptions of analyzed zircons, concordia diagrams, and CL images are shown in the Supplemental Material and Figure S1. Isotopic data are given in the Supplementary Material (Table S3). The U-Pb ages of igneous zircon defined two sequential age groups: (1) a Cretaceous group, including diorite, granodiorite, tonalite, and granite plutons, ranging from ca. 142 to 90 Ma and displaying a wide range of Th/U (0.2–2.38), and (2) a Tertiary group, comprising diorite, tonalite, and gabbro plutons ranging from ca. 34 to 4 Ma and with a wide range of Th/U (0.12–2.19). Only 2% of analyses represented inherited zircon crystals distributed in a diorite (ca. 608, 607, 497, 123, 120 Ma), a gabbro (ca. 120, 119 Ma), and a granodiorite-tonalite (ca. 366, 362, 356 Ma), indicating recycling of Neoproterozoic, Paleozoic, and Cretaceous sources. After integrating the ages from the Aysén and Bariloche sections (Figs. 1A and 1B), three main peaks of plutonic activity at 168, 121, and 12 Ma were identified in the North Patagonian batholith.

KINEMATIC ANALYSIS OF LITHOSPHERIC PLATES

Determination of the linear velocities of the Farallon-Nazca (breakup of Farallon to Cocos and Nazca plates took place at around 25–23 Ma), Phoenix-Aluk (hereafter called Aluk), and Antarctic plates relative to the South American plate during the last 180 m.y. was performed following standard procedures of plate kinematic analysis. Relative velocity vectors were determined at a line of points located along the Chile Trench in the segment between 38°S and 55°S, at 1° intervals and taking South America as the fixed plate. Special emphasis was placed on the zone corresponding to the North Patagonian batholith (39°S to 46°S). The relative angular velocity vectors of the involved plates were obtained from distinct sources from the literature (see references in the caption to Fig. 6). Determination of the 3 × 3 matrices of total reconstruction rotations was directly derived from the compiled data. Following the rules of finite rotations (Cox and Hart, 1986), the matrices of forward motion stage rotation were determined. For each stage, the angular velocity vector from 70 Ma to 0 Ma, with intervals of 5 m.y., was obtained. From that information, standard procedures allowed computation of the relative linear velocity vectors at each studied site along the Chile Trench. In the case of the displacement of Aluk relative to South America, finite rotation matrices describing the relative displacement of these two plates are not available. Therefore, it was necessary to use the "absolute" motions of Aluk and South America relative to a hotspot reference frame (HS) for the period between 64 Ma and 0 Ma to obtain the total reconstruction rotations of Aluk relative to South America. The rest of the procedure matches the one used for the rotation of Farallon/Nazca versus South American plates. The period between 180 and 85 Ma lacked data for some time intervals (Engebretson et al., 1985). The need to obtain information every 5 m.y. forced us to determine those rotations by calculating the intermediate rotation matrices. The remaining procedure was identical to that explained for the period 64–0 Ma. No information was found for the period 85–60 Ma.

The kinematic analysis presented here does not differ from previous studies regarding the nature of the methodology used to obtain the relative velocity vectors of the different subducting plates with respect to the South American plate. However, there are two aspects that make the approach presented in this work novel. First, a long period of time was modeled (the last 180 m.y.), while previous studies tended to focus on specific stages of the evolution of the Andean margin. Second, the variation in the relative velocity vectors between the plates over a large segment of the margin (between 38°S and 55°S) was analyzed in great detail (1° intervals). In previous studies, the interest had focused on the determination of vectors of average relative velocity or in much less extensive areas, without the coverage that has been given in this work. Because both the methodology and the databases used here and in other works are the same, the results for specific points of the margin and for specific periods of time are very similar to those previously published by other authors (e.g., Haschke et al., 2006a; Pardo-Casas and Molnar, 1987; Somoza, 1998; Somoza and Ghidella, 2012). However, the approach presented in this work is the only one that allows a detailed comparison between the tectonic setting in terms of relative plate motions and the geochemical and geochronological evolution of the North Patagonian batholith, which was the objective of this study.

The kinematic evolution of lithospheric plates that were involved in the generation of the North Patagonian batholith is shown in Figure 6 for the four main periods of magmatic activity. Starting with the oldest stages of

tectonic evolution (ca. 180 Ma), subduction velocities of the Aluk plate were high (>>140–150 km m.y.$^{-1}$) and predominantly normal to the trench (α = 60°–70°, where α is the obliquity angle, i.e., the angle between the velocity vector and the azimuth of the trench) in the period 180–140 Ma (Fig. 6, stage 1). At 140–130 Ma, a strong decrease down to 90–100 km m.y.$^{-1}$ (Fig. 6, stage 2) in the convergence velocity coincided with similar to slightly lower α values (50°–70°). Velocity values progressively increased during the period 130–100 Ma, while the obliquity angle attained 80°. A new change took place between 100 and 85 Ma, with very low relative velocities (<40 km m.y.$^{-1}$) of nearly orthogonal convergence. Kinematic information is lacking for the period 85–60 Ma. The last segment of Aluk was subducted below the South America plate between 60 and 50 Ma, with velocities of 70–80 km m.y.$^{-1}$ and moderate obliquity angles (50°–60°). The available information suggests that the Farallon–Aluk–South America triple junction quickly migrated from north to south along the North Patagonian batholith between ca. 50 and 45 Ma (during stage 3, Fig. 6). Subduction of the Farallon plate started at ca. 45 Ma in the studied area, with convergence velocities and angles similar to, albeit slightly lower than, that of the last stage of subduction of Aluk (Fig. 6, initial stage 4). A marked increase (up to 140 km m.y.$^{-1}$) of subduction velocity happened during the Oligocene at around 30 Ma, also with a high obliquity angle of >80° (Fig. 6, plain stage 4). The kinematic history during the last 20 m.y. (Fig. 6, 15 and 0 Ma) shows a progressive decrease of the relative velocity (70–80 km m.y.$^{-1}$ currently) and of the obliquity angle (present values are α = 80°). The Nazca–Antarctic–South America triple junction is slowly migrating northward, and it is currently located at the contact between the South and North Patagonian batholiths. Therefore, neither the triple junction nor the subduction of the Antarctic plate has affected the studied zone.

In sum, four main tectonic stages can be identified according to the kinematic regime (Figs. 6 and 7): (1) Jurassic, (2) Early Cretaceous, (3) Late Cretaceous–Paleogene, and (4) Neogene–Quaternary. Interestingly, we report clear differences in the rate of magma production (volume addition rate per arc length; Fig. 7A): ~4 km^3 m.y.$^{-1}$ km^{-1} for the older stages 1 and 2 (Jurassic to Early Cretaceous), ~10 km^3 m.y.$^{-1}$ km^{-1} in stage 4 (Neogene), and very low values during stage 3 (Late Cretaceous–Paleogene, ~0.5 km^3 m.y.$^{-1}$ km^{-1}), which was characterized by episodes of null magmatic activity. These tectonic stages were checked for changes in the source compositions of magmas identified on the basis of their Sr-Nd initial isotopic fingerprints.

DISCUSSION

In Andean (= Cordilleran) batholiths, the origin of granites is a controversial matter. The melting of the lower crust and fractionation from a basic magma precursor followed by crustal assimilation are in principle able to produce granitic magmas. The two opposite hypotheses account for the hybrid (crust + mantle) composition of granitic batholiths. However, the way magmas acquire these crustal components is debated.

On one hand, isotopically evolved components (e.g., older crust and sediments) may be introduced into the mantle by subduction (Stern, 1991a, 1991b). On the other hand, pristine mantle magmas may acquire evolved components in the continental crust by processes of magma assimilation, storage, and hybridization (MASH; Hildreth and Moorbath, 1988). The two processes are discussed in this section in light of geochemical and geochronological data obtained from the North Patagonian batholith.

Crustal Origin: Melting, Assimilation, and MASH

The systematic presence of isotopically evolved features in Andean-type batholiths, and in arc magmas in general (DePaolo, 1981a), is traditionally attributed to crustal assimilation. The correlation between the thickness of the crust and the evolved isotopic ratios (high $^{87}Sr/^{86}Sr$ and low $^{143}Nd/^{144}Nd$) in volcanic rocks of central Chile was the basis for the MASH (melting, assimilation, storage, and hybridization) hypothesis (Hildreth and Moorbath, 1988). However, the application of the MASH model to account for the geochemical variability of plutons entails serious difficulties. First, the secular geochemical variations observed for long periods of time are not compatible with the expected decrease of crustal contaminants in a protracted process of assimilation. Second, there is no clear correlation between major-element compositions and evolved isotopic ratios (Nielsen and Marschall, 2017; Stern, 2020). Although a positive correlation between silica and the Sr isotopic ratio has been found in some lavas of the Andean Central volcanic zone (Davidson et al., 1991), other Andean volcanic centers show a scattered distribution or a constant Sr initial ratio for a wide range of silica content in lavas (Davidson et al., 1991). Moreover, constant Nd initial ratios have been reported in Andean plutonic and volcanic rocks covering a wide range of silica from 50 to 75 wt% (Stern, 2020, his fig. 11). A process of assimilation and fractional crystallization (AFC) will produce a trend with changing initial isotopic ratios with magma composition (DePaolo, 1981b). Third, the geochemical trends (major elements) of plutons closely follow the differentiation cotectic lines and not the assimilation trends (see review in Castro, 2013). In the case of the North Patagonian batholith, assimilation trends pointing to metasediments are not observed, and the radiogenic ratios for Sr and Nd isotopes are equally found in diorites and granites. Moreover, the lack of inherited cores in most samples implies a single magmatic cycle for the origin of zircon and the absence of local assimilation in the crust during ascent and emplacement of plutons.

Andean-type batholiths could have been generated by melting of a hybridized lower crust (Hammerli et al., 2018). Although this mechanism can account for hybrid isotopic features, high melt fractions are required to produce tonalites and granodiorites from a hybrid crustal source, implying very high temperatures around 1000–1100 °C at lower-crustal pressures (1–1.5 GPa) according to experimental data (Castro et al., 2010). These temperatures are higher than those predicted by thermal models, even when high proportions of basaltic sills were emplaced at the lower crust (Annen and Sparks, 2002).

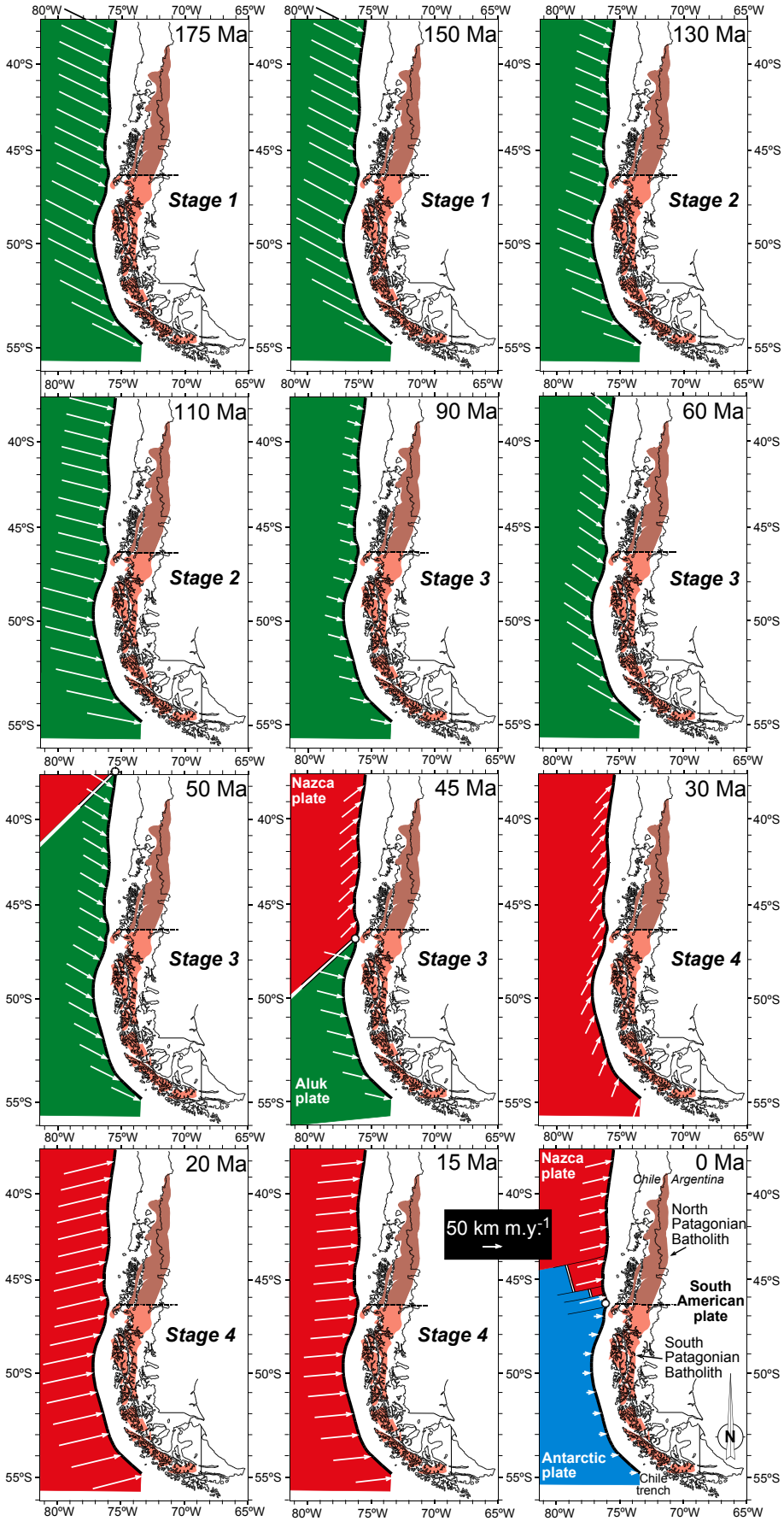

Figure 6. Reconstructed Aluk, Nazca, and Antarctic plate motions relative to a fixed South American plate. Although the entire time period spanning from 180 Ma to 0 Ma has been studied, only 12 selected snapshots are shown here, representative of the four evolution stages mentioned in the main text. The maps show, using Universal Transverse Mercator (UTM) projection, the present-day Chilean and Argentinian coastlines and the trench contour. The triple junctions are represented when it is required. The computed velocity vectors are plotted at scale on the moving plates and located along the trench, with 1° spacing. The data sources are as follows: displacement of Nazca relative to South America (DeMets et al., 2010; Somoza and Ghidella, 2012); displacement of the Antarctic plate relative to South America (Cande and Leslie, 1986; DeMets et al., 2010); displacement of Aluk relative to South America (Engebretson et al., 1985; Gordon and Jurdy, 1986); displacement of triple junctions relative to South America (Cande and Leslie, 1986; Somoza and Ghidella, 2012). Computation of the relative velocity vectors followed the rules of finite rotations (Cox and Hart, 1986). Concerning the novelty of the convergence directions relative to those calculated elsewhere, see the main text.

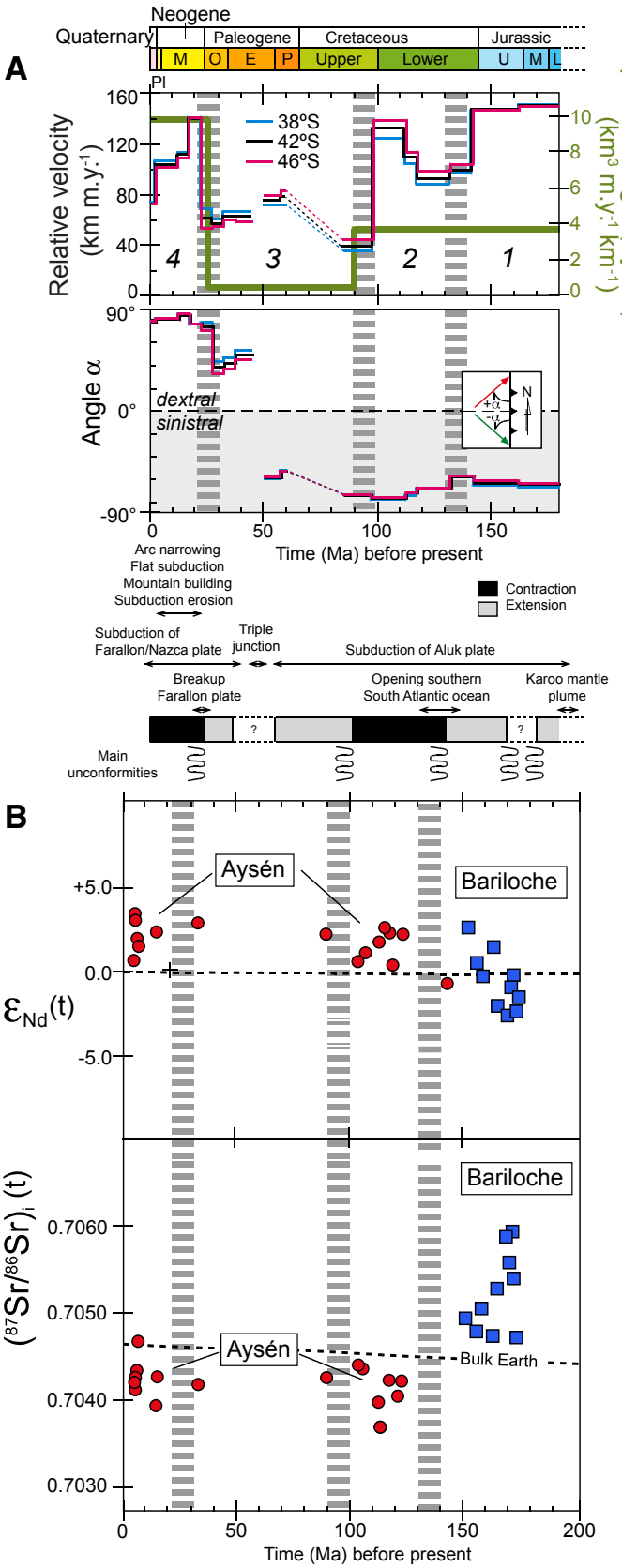

Figure 7. Summary of plate kinematics data and correlations with Sr and Nd initial isotopic ratios of plutons. (A) Time variation of plate velocities computed for the displacement of the Aluk (before 50–40 Ma) and Nazca (after 50–40 Ma) plates relative to the South American plate at three selected latitudes, corresponding to the northern (38°S) and southern (46°S) boundaries of the North Patagonian batholith and its central line (42°S). Angle α is convergence obliquity (α = 0° for parallel and α = 90° for orthogonal relative displacement). Positive/negative values refer to dextral/sinistral convergence. Approximate volume addition rate per arc-length of plutonic rocks at Aysén was calculated based on map relative surfaces, a N-S length of 200 km, and considering an average depth of 10 km for the batholith according to models (Cruden et al., 2018). Age bins are large due to the scarce number of available age determinations at the studied zone. Values are apparently lower than typical arc magma production rates (e.g., Wörner et al., 2018), first, because of the bin size and, second, due to the fact that the volcanic rocks and the lower-crust intrusions have not been considered. In any case, the time variations of the addition rate shown by the upper-crust batholith have a very clear expression, regardless of similar variations in the contemporary volcanism or magma emplacement at the lower crust. Relevant tectonic events in the South American plate (Echaurren et al., 2017; Folguera and Iannizzotto, 2004; Haschke et al., 2006b; Orts et al., 2012) are also shown. Numbers 1 to 4, separated by thick, vertical, dashed gray lines, mark the four evolutionary stages identified in this work. U—Upper; M—Middle; L—Lower. (B) Initial isotopic ratios of $^{87}Sr/^{86}Sr$ and $^{143}Nd/^{144}Nd$, the latter in epsilon notation, for dated samples of the North Patagonian batholith, calculated at the time (*t*) of magma generation. Numbers 1 to 4, separated by thick, vertical, hashed gray lines, mark the four evolutionary stages identified in this study. M—Miocene, O—Oligocene, E—Eocene, P—Paleocene.

Water-assisted melting of lower-crust sources (Qian and Hermann, 2013) may proceed at lower temperatures, giving rise to water-saturated granitic liquids. This is in contradiction with the characteristic water-undersaturated conditions that prevail during crystallization of magmas in the upper crust. In sum, although crustal signatures are implicit in Andean-type batholiths, a crustal origin for magmas is very unlikely.

Fractionation from a Dioritic (Andesitic) Parental Magma

A plausible interpretation, as an alternative to crustal melting and assimilation, is fractionation from a mafic magma precursor coming from the subduction system and carrying crustal signatures. The composition of this mafic precursor has been widely debated. Models based on a basaltic composition have failed to explain the geochemical features of magmas and the scarcity of ultramafic residues in the lower (arc) crust. By contrast, the "andesite model," which was introduced by S.R. Taylor years ago (Taylor, 1967), accounts for liquid compositions (diorites and granodiorites) in Cordilleran batholiths (Castro, 2013, 2020; Castro et al., 2010, 2013). Moreover, major-element trends of arc volcanics and calc-alkaline batholiths follow curved linear patterns (for review, see Castro, 2020), which are compatible with liquid lines of descent relating to intermediate (andesitic) parental compositions as the precursors of batholiths.

Accordingly, proxy diagrams (Fig. 8) plotting major oxides, for which variations are controlled by phase relations, were used here to reveal the main process responsible for geochemical variations in the North Patagonian batholith. Rock compositions plot along the low-water main cotectic array of calc-alkaline systems, which was traced from experiments using a modeled parental intermediate magma (Castro, 2020, 2021). This parental magma has a dioritic composition (with SiO_2 = 58.6 wt%, FeO = 7.3 wt%, MgO = 3.2 wt%, CaO = 6.5 wt%, K_2O = 1.5 wt%), and it was determined by two independent approaches: (1) near-solidus experiments on lower-crust granulites, assumed to be cumulates formed in the course of fractionation to granitic melts; and (2) the composition of the gap observed in the Patagonian batholith. The following observations arise from the comparison between the experiments and North Patagonian batholith samples (Fig. 8): (1) Those rocks richer in silica (SiO_2 >63 wt%) follow a pattern that is on average very similar to the low-water cotectic array. (2) Diorites and quartz-diorites (SiO_2 <63 wt%) plot in an area overlapping Pl-Px solid residues, which belong to the same experiments that yielded the cotectic liquids.

These comparisons extend to the whole Patagonian batholith to emphasize that interpretations from the Aysén and Bariloche regions of this study are not local and can be of general applicability. The low-water cotectic array, mentioned above, is compared with the composition of the whole Patagonian batholith in Figure 9. Other cotectic trends resulting from high-water experiments are also shown for comparison (Fig. 9A). It is clear that low initial water conditions prevailed in the batholith parental magmas. The low-water cotectic line was traced from experimental liquids at conditions of 0.3 and

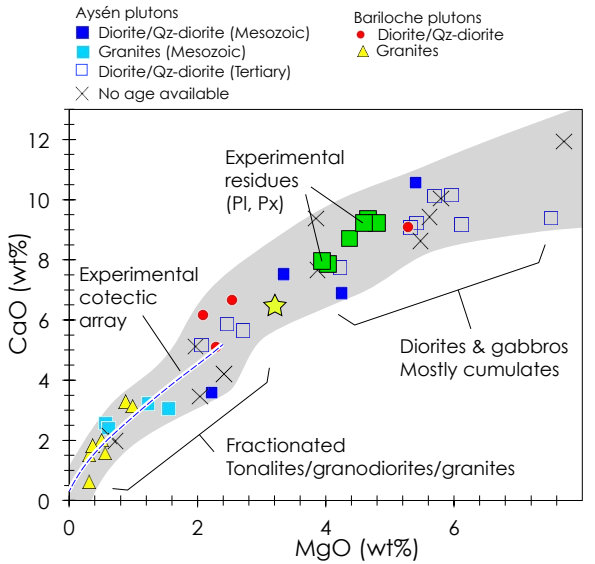

Figure 8. CaO-MgO diagram (wt%) showing the North Patagonian batholith samples compared with the low-water cotectic array and their corresponding plagioclase-pyroxene (Pl-Px) solid residues (details on this array are given in Fig. 9). Yellow star marks the composition of model parental magmas for calc-alkaline batholiths (Castro, 2020) (see text for additional explanation). Qz—quartz.

1 GPa and 1100–800 °C (Fig. 9B) using a modeled diorite composition as the starting material (yellow star in Fig. 9A). Diorites and gabbros with higher MgO and CaO contents may represent cumulates. In fact, many of these diorites and gabbros often overlap lower-crust granulitic compositions. This supports the inference that diorites-gabbros are related by a fractionation process similar to that connecting granites and granulites on a wider scale. Furthermore, liquid and bulk solid compositions are very similar at 0.3 and 1 GPa (Fig. 9), implying that lower- and upper-crust differentiation processes can give similar results. There is a significant gap along the cotectic, also reproduced by experiments, that supports fractionation as the main process relating granitic rocks (mostly granodiorites) and quartz-diorites. The two groups are marked by two kernel density maxima in the CaO-MgO diagram (Fig. 9B) and coincide with experimental liquids at 1050 °C and 1000 °C, at 0.3 GPa. A big jump in composition within a 50 °C margin is parallel to an increase in liquid percentage from 38 wt% at 1000 °C to ~60 wt% at 1050 °C (see inset in Fig. 9B), a phenomenon considered intrinsic to fractionation of arc magmas (Reubi and Blundy, 2009).

These data support the interpretation that granitic rocks (SiO_2 >63 wt%) of the Aysén and Bariloche regions represent fractionated liquids from a

common parental intermediate magma of dioritic composition. Most diorites and some scarce gabbros with low silica and low MgO contents (Fig. 8) may represent cumulates, i.e., crystal mushes that lost a residual granitic liquid during crystallization. A discussion on the mechanism of crystal/liquid separation is out of the scope of this paper. Separation of a crystal-rich mush and a fractionated liquid (magmatic splitting) is intrinsic to crystallization at the thermal boundary layers of ascent conduits (Rodríguez and Castro, 2017). Crystallization experiments and the mechanical behavior of magmas in conduits, where mafic microgranular enclaves are generated (Fernández and Castro, 2018), support magma splitting as a mechanism responsible for crystal/liquid segregation. Such magmatic enclaves are common features to all Andean batholiths, and their presence proves two essential aspects that must be considered in addressing petrogenetic interpretations of batholiths. First, they represent early magma pulses that quenched against the ascent conduits, which supports a near-liquid state of the magmas. Second, they are indicators of magmatic fractionation leading to differentiation during ascent and emplacement of plutons. Trace elements also support magma fractionation as the process linking diorites and granites in the North Patagonian batholith (Castro et al., 2011). Fractionation of REEs is compatible with fractionation of solid assemblages dominated by clinopyroxene and plagioclase.

Amphibole thermometry and hygrometry (measurement of the liquid water content in equilibrium with amphibole) constitute relevant data because they can be used to constrain the origin of magmas. In accordance with textures, which reveal amphibole crystallization in late magmatic stages in dioritic and granitic rocks (Figs. 2E–2H), amphibole temperatures yielded values below 800 °C (Fig. 5). These temperatures are near-solidus in diorites, implying that amphibole started to precipitate in dioritic magmas when the crystal content was higher than 60 wt%, which is in total agreement with textural observations. A comparison was made with the curve at 60 wt% of crystals, calculated with Rhyolite-MELTS from a diorite with 2 wt% initial water content (Fig. 5). The results were consistent with hygrometric estimates, which clustered at ~5–6 wt% water and 780–810 °C, supporting the supposition that an initial water content of ~2 wt% would have been sufficient to reach the necessary conditions for amphibole crystallization at later stages. Amphibole crystals formed at lower temperatures yield higher melt water contents (Fig. 5), which is compatible with water enrichment in the residual melt of a crystallizing magma. In our case, low-temperature amphiboles formed near the solidus of the water-saturated granite minimum (Fig. 5), with some of them being subsolidus actinolites. In the case of the Bariloche area, where granitic rocks are dominant, amphibole temperatures were also near the solidus, which implies low initial water content in the magmas. Near-solidus crystallization of amphibole, which is a characteristic feature of Andean-type batholiths (Castro, 2013), is also supported by the common pyroxene-to-amphibole replacement textures as a consequence of rehydration of the residual liquid (Beard et al., 2004). Also, the presence of polycrystalline amphibole aggregates (clots) provides evidence of late magmatic (near-solidus) pyroxene destabilization and replacement (Castro and Stephens, 1992).

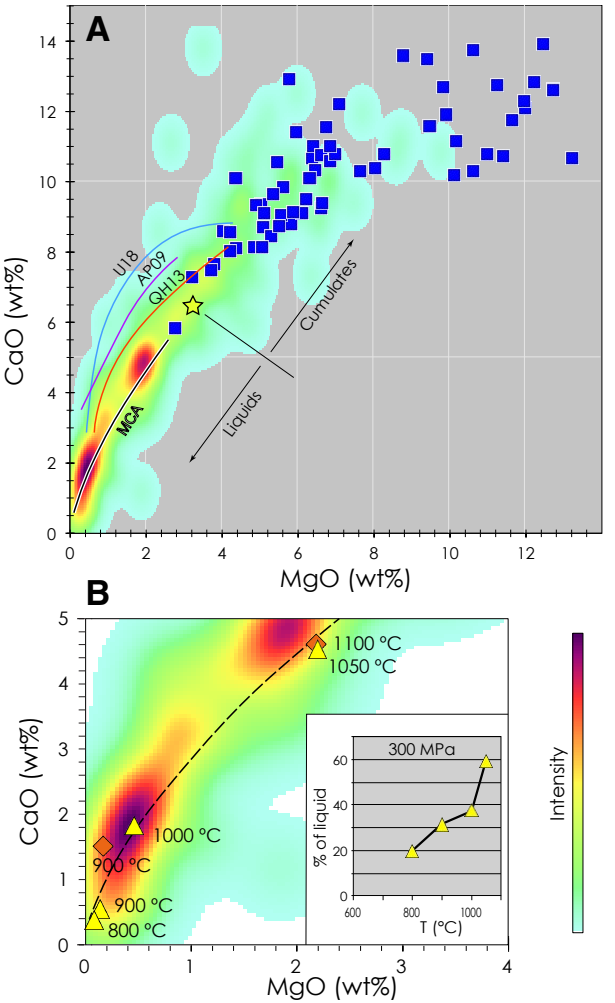

Figure 9. Diagrams showing the comparison of experimental data with the overall composition of the Patagonian batholith. (A) Kernel density plot of the Patagonian batholith (238 samples) compiled from the literature (see Castro, 2020). Cotectic arrays from high-water-content and low-water-content experiments are also shown. These are: U18 (Ulmer et al., 2018); AP09 (Alonso Perez et al., 2009); QH13 (Qian and Hermann, 2013); MCA (main cotectic array; Castro, 2021). The region of cumulates overlaps with many lower-crust granulites (blue squares). (B) Detail of the granitic (sensu lato) region of the former diagram showing the 1 wt% water cotectic array (MCA) traced after the compositions of experimental liquids at 300 MPa (yellow triangles) and 1 GPa (orange diamonds; Castro, 2021). The compositional jump between the two maxima takes place within the range of 50 °C at 300 MPa and corresponds with the jump in liquid fraction (inset in B). Yellow star in A represents the dioritic parental composition. Kernel density values were computed using the generic function density in R code. For further explanation, see main text.

Magma Sources

A parental intermediate magma was identified by experimental constraints. Next, we addressed the problem of the source of the magmas by means of Sr and Nd systematics. In the North Patagonian batholith, a wide range of isotopic ratios is found in plutons, irrespective of whole-rock compositions. Initial isotopic ratios for $^{87}Sr/^{86}Sr$ and $^{143}Nd/^{144}Nd$ of selected samples from the North Patagonian batholith were normalized to the age of generation in three groups, 168, 121, and 12 Ma, according to the three main peaks of magmatic activity (Fig. 10).

The two end members of crustal components in the mélange (Fig. 11) correspond to the midpoints on the fields of the Chilean accretionary complex and the North Patagonian massif (Pankhurst et al., 1999). These two midpoints were recalculated in accordance with the three peaks of magmatic activity at 168, 121, and 12 Ma (Fig. 11), assuming the modeled compositions for Rb, Sr, Sm, and Nd of the bulk continental crust (Rudnick and Gao, 2003) for the North Patagonian massif, and global subducting sediment (GLOSS; Plank and Langmuir, 1998) for the Chilean Trench sediments.

Whatever the nature of crustal sources involved (sediments or Neoproterozoic basement), recycled isotopic fingerprints are present in both diorites and granites, indistinctively. For instance, the most primitive diorite [sample A208–11: ε_{Nd} = 1.34; $(^{87}Sr/^{86}Sr)_i$ = 0.70469] from Bariloche (Fig. 11A) is richer in silica (62 wt%; Table 1) than the less primitive diorite [sample A208–14: ε_{Nd} = –2.66; $(^{87}Sr/^{86}Sr)_i$ = 0.70582]. Because crustal assimilation will tend to increase the silica content of the most contaminated magma, the observed decoupling is likely to be compatible with variable proportions of sediments in the source (Vogt et al., 2013). It has been experimentally shown (Castro et al., 2010) that magma composition can be buffered over a wide range of end members in a composite source (mélange).

These are features of premelting mixing of subducted mélanges (Nielsen and Marschall, 2017). All plutons, felsic and mafic, plot along mixing lines (Fig. 11) linking the altered oceanic crust and the two crustal sources available in the region, namely, the inferred Mesoproterozoic basement of the North Patagonian massif and sediments of the Chilean accretionary complex (Pankhurst et al., 1999). The magma source in Bariloche was a mélange composed of basement and altered oceanic crust, with the fraction of altered oceanic crust (X_B) ranging from 0.6 to 0.3 (Fig. 11A). In the Aysén region, the altered oceanic crust fraction of plutons is higher, i.e., X_B = 0.8–0.6 (Figs. 11B and 11C), and the continental component is in part represented by sediments of the accretionary complex. The youngest plutons (12 Ma) plot between the two mixing curves, supporting the implication of a mélange formed by trench sediments, altered oceanic crust, and old crustal basement in the source region of the magmas. The three end members could have been introduced via subduction erosion (von Huene and Schöll, 1991) and sediment subduction into the subduction channel (Cloos and Shreve, 1988), where they mixed mechanically and evolved into Rayleigh-Taylor instabilities and diapiric structures intruding into the hot neighboring mantle (Gerya and Yuen, 2003; Gerya et al., 2004; Marschall and Schumacher, 2012), where conditions favorable for melting existed. Experimental works on mélange melting (Castro et al., 2010; Cruz-Uribe et al., 2018) showed that temperatures >1000 °C are required to satisfy melt compositions and involved phase equilibria. About 50 vol% liquid of granodioritic composition can be formed at T = 1050–1100 °C and P = 1.5–2.0 GPa (Castro et al., 2010) from an amphibolite-pelite mélange. The production of less silicic magmas, like the diorites forming large plutons in the North Patagonian batholith, requires either the incorporation of crystals from the source or an increase in the melt fraction by raising the temperature to near-liquidus conditions (>>1200 °C). In the latter case, a complete reaction of the mélange with the peridotite is the most suitable scenario leading to the generation of wet dioritic liquids in equilibrium with forsteritic olivine (Castro et al., 2013).

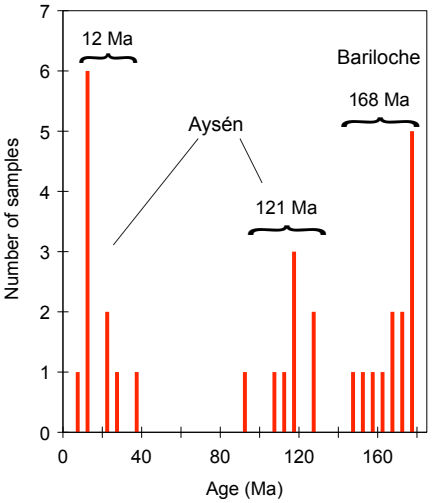

Figure 10. Age-frequency histogram showing the three main peaks of plutonic activity in the North Patagonian batholith at 168, 121, and 12 Ma.

Geodynamic Implications

According to thermomechanical models (Gerya and Meilick, 2011; Vogt et al., 2012), the proportions of end members in the mélange are dictated by tectonic parameters such as the subduction angle, convergence rate and obliquity, and the thermal-mechanical state of the lithosphere. In this way, the correlation between tectonic processes and magma isotope composition can be found, which supplies an additional proof for the mélange diapir model (MDM). Such correlation is found in the North Patagonian batholith as follows:

(1) High relative linear velocities (~140 km m.y.$^{-1}$) and obliquity angles (60°–70°) predominated in the age interval ca. 180–140 Ma (stage 1, Fig. 12A) due to the subduction of Aluk below South America. The Jurassic kinematics were dominated by the extensional tectonic regime in the South America

Figure 11. (A–C) Mixing models of initial isotopic ratios of Sr and Nd (Nd in epsilon ε notation), showing possible mélange source compositions using a juvenile end member, represented by the altered oceanic crust (AOC), and two evolved end members, represented by the North Patagonian massif and the Chilean accretionary complex. These are compared with isotopic ratios of plutons normalized to the three peaks of plutonic activity at 168, 121, and 12 Ma. Squares along the mixing lines represent 10% increments of end members involved. Qz—quartz.

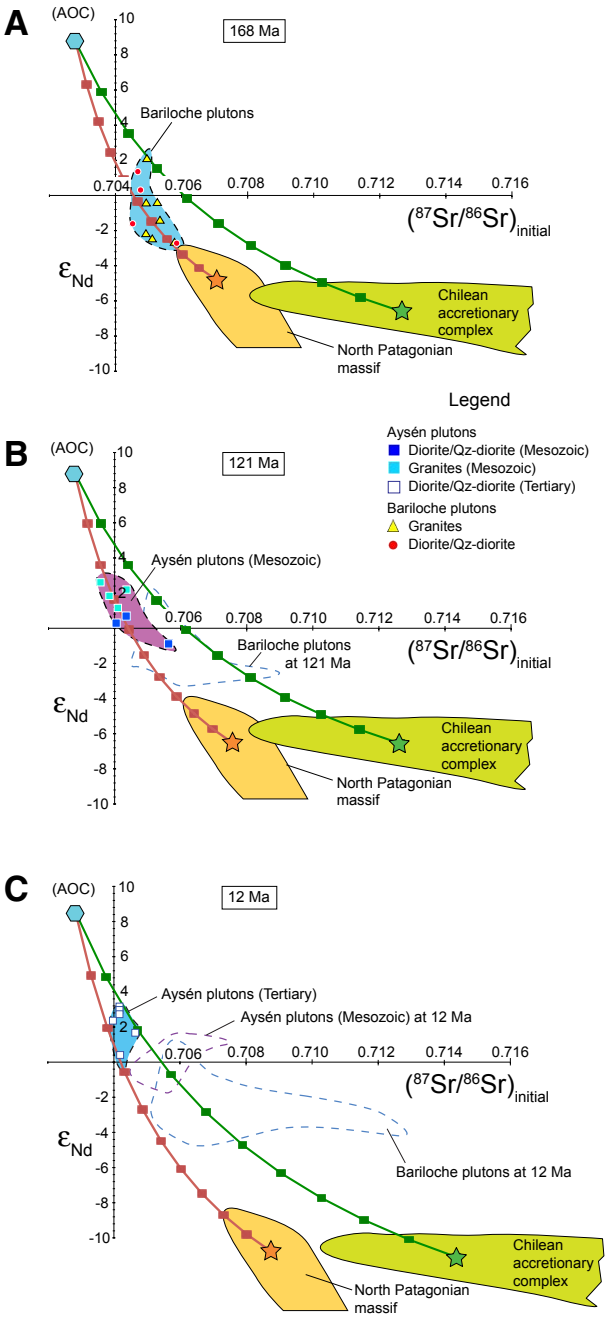

plate (Echaurren et al., 2017), fast plate convergence (~140 km m.y.$^{-1}$), and sparse sediment supply, which are all considered to be favorable conditions for subduction erosion (Clift and Vannucchi, 2004; Keppie et al., 2009), leading to the entrainment into the mantle of materials from the upper-plate basement (Stern, 2011). Plutons of the North Patagonian batholith (diorites and their derivative granites) that formed during stage 1 record old crustal signatures (high initial $^{87}Sr/^{86}Sr$ and very negative ε_{Nd}; Figs. 7B and 11A) compatible with the implication of a Mesoproterozoic basement in the source.

(2) A sudden drop in the relative velocities of Aluk (down to 90–100 km m.y.$^{-1}$) marks the Jurassic-Cretaceous transition. The Early Cretaceous (stage 2; Figs. 6, 7A, and 11B) was characterized in the region by a progressive increase in the velocity of convergence, triggered by the opening of the southern South Atlantic Ocean (Franke, 2013; Larson and Ladd, 1973). Obliquity angles attained 80°, giving rise to a period of plate coupling that favored subduction of trench sediments (Vogt et al., 2012, 2013), formed by denudation of the previously formed arc. Subduction erosion of the Proterozoic basement may have continued during this stage, giving rise to a three-component mélange. Some plutons of the North Patagonian batholith plot between the two mixing curves in Figure 11A, denoting the influence of subducted sediments in the source of magmas (see also Fig. 7B).

(3) Relatively slow convergence velocities (around 60 km m.y.$^{-1}$), low obliquity angles (40°–60°), and extensional or transtensional tectonic conditions (e.g., Folguera and Iannizzotto, 2004; Haschke et al., 2006b) characterized the Late Cretaceous and Paleocene (stage 3; Figs. 6, 7A, and 11C). The low convergence rates, typical of stage 3, together with the switch to extensional conditions and low rates of sediment arrival to the trench are conditions favoring the absence of subduction erosion (Clift and Vannucchi, 2004). These features explain the low magmatic productivity of this period (~0.5 km^3 m.y.$^{-1}$ km^{-1}; Fig. 7A).

(4) The last tectonic episode (stage 4, Fig. 12D) commenced upon the breakup of the Farallon plate (Lonsdale, 2005) at ca. 25–23 Ma and the abrupt increase in the velocity of Nazca relative to South America, restoring values of around 140 km m.y.$^{-1}$ at nearly orthogonal convergence (>80°). Accordingly, a contractional regime dominated this stage along with arc narrowing and mountain building (Haschke, et al., 2006a; Orts et al., 2012).

(5) The most recent kinematic evolution shows a progressive decrease in the convergence velocities down to around 80 km m.y.$^{-1}$, which coincides with current values (DeMets et al., 2010). The tectono-magmatic conditions were similar during stages 2 and 4 (Figs. 6, 7, and 11). Therefore, Miocene to

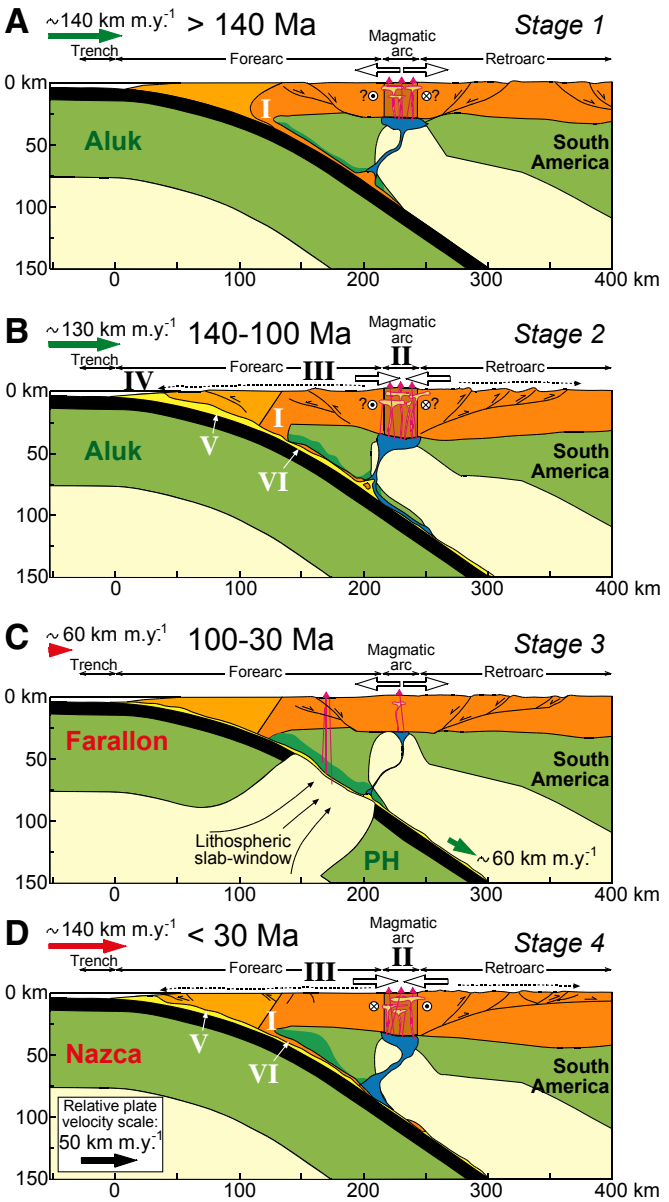

Figure 12. (A–D) Plate profiles depicting the lithosphere sections for the main evolutionary stages during the generation of the North Patagonian batholith. The sections integrate magma sources according to isotopic ratios of plutons and plate-tectonic evolution over the period ca. 180–10 Ma. The location of mélange diapirs and plate geometry follow results of thermomechanical numerical models (Gerya and Meilick, 2011; Gerya and Yuen, 2003; Vogt et al., 2012, 2013). SA—South America; PH—Phoenix plate.

recent magmas show juvenile isotopic ratios (Fig. 7B), with more than 80% altered oceanic crust and coupled participation of the two continental reservoirs, namely, the inferred Proterozoic basement and subducted sediments.

Taking into account the results of this study and experimental constraints, it follows that secular changes in magma source compositions are fairly well correlated with changes in tectonic processes during subduction and justified by models and on geophysical grounds. For instance, coupling periods of subduction enhance subduction erosion of the upper plate (von Huene and Schöll, 1991) and introduce low-density portions of the continental crust into the subduction channel (Gerya and Yuen, 2003). Thermomechanical models of subduction zones (Gerya et al., 2004; Vogt et al., 2012) predict an alternation between coupling and decoupling stages over periods of several million years, which are recorded by changes in the isotopic signatures of magmas (Vogt et al., 2013). Another prediction of the models is the secular change in the proportions of end members incorporated into the subduction channel in response to changes in the rheology of the suprasubduction lithosphere (Gerya and Meilick, 2011).

CONCLUSIONS

The correlation found between tectonic processes, necessary to drag crustal materials down to the depth of the mantle, and the petrological and geochemical features of magmas during the period of batholith amalgamation is crucial to understand the origin of magmas that formed the North Patagonian batholith.

The close similarities among intermediate magma precursors (diorites) and their derivative granites are the general feature of the North Patagonian batholith, in which plutons were formed and emplaced over ~170 m.y. Remarkably, plutons sharing close major-element compositions have important differences in terms of Sr and Nd isotopic ratios, with implications for distinct sources with varied crustal residence times. Since these isotopic differences are found in the diorite precursors, the crustal imprints must have been acquired at the source of the magmas in the mantle rather than in the continental crust. Trace elements display variable ratios, as these are the sum of source composition and fractionation in the upper crust (see our former paper on the Bariloche area, Castro et al., 2011). Isotopic ratios (Sr and Nd in this study) are not affected by crustal differentiation of magmas. Thus, they can be used to monitor source-related processes (e.g., proportion of crustal components in the mélange).

The parental diorite precursor that arrived to the arc crust and fractionated to form the batholiths could have been in turn fractionated from a more mafic melt of basaltic andesite composition, which formed within the mantle by complete reaction of the bulk mélanges and the peridotite.

We conclude that the time-ordered changes in source-related signatures in batholiths over protracted periods of time and their correlations with tectonic evolution are fundamental to support the mélange diapir model for magma generation based on melting of subducted mélanges. According to isotopic ratios, a large proportion (>50%) of oceanic crust, representing juvenile material in batholiths, is recycled into new arc crust in subduction zones.

We propose that the parental mafic to intermediate magmas that gave rise to the plutons and batholiths were rooted below the lithosphere of the overriding plate. In this model, distinct isotopic reservoirs, depending on the tectonic regime and available materials, can be incorporated via subduction and subduction erosion.

ACKNOWLEDGMENTS

This research was funded by the Spanish Agency of Science and Technology (Projects CGL2013–48408–C3–1–P and PGC2018–096534-B-I00) and the University of Huelva. Rodriguez is grateful for a Juan de la Cierva postdoctoral research grant. This is IBERSIMS publication 49.

REFERENCES CITED

Alonso Perez, R., Müntener, O., and Ulmer, P., 2009, Igneous garnet and amphibolite fractionation in the roots of island arcs: Experimental constraints on andesite liquids: Contributions to Mineralogy and Petrology, v. 157, p. 541–558, https://doi.org/10.1007/s00410-008-0351-8.

Annen, C., and Sparks, R.S.J., 2002, Effects of repetitive emplacement of basaltic intrusions on thermal evolution and melt generation in the crust: Earth and Planetary Science Letters, v. 203, p. 937–955, https://doi.org/10.1016/S0012-821X(02)00929-9.

Aragón, E., Castro, A., Díaz-Alvarado, J., and Liu, D.-Y., 2011, The North Patagonian batholith at Paso Puyehue (Argentina-Chile): SHRIMP ages and compositional features: Journal of South American Earth Sciences, v. 32, no. 4, p. 547–554, https://doi.org/10.1016/j.jsames.2011.02.005.

Baedecker, P.A., 1987, Methods for Geological Analysis: U.S. Geological Survey Bulletin 1770, 187 p.

Bea, F., 1996, Residence of REE, Y, Th and U in granites and crustal protoliths: Implications for the chemistry of crustal melts: Journal of Petrology, v. 37, no. 3, p. 521–552.

Beard, J., Ragland, P.C., and Rushmer, T., 2004, Hydration crystallization reactions between anhydrous minerals and hydrous melt to yield amphibole and biotite in igneous rocks: Description and implications: The Journal of Geology, v. 112, p. 617–621, https://doi.org/10.1086/422670.

Black, L.P., Kamo, S.L., Allen, C.M., Aleinikoff, J.N., Davis, D.W., Korsch, R.J., and Foudoulis, C., 2003, TEMORA 1: A new zircon standard for Phanerozoic U-Pb geochronology: Chemical Geology, v. 200, no. 1, p. 155–170, https://doi.org/10.1016/S0009-2541(03)00165-7.

Cande, S.C., and Leslie, R.B., 1986, Late Cenozoic tectonics of the southern Chile Trench: Journal of Geophysical Research, v. 91, no. B1, p. 471–496, https://doi.org/10.1029/JB091iB01p00471.

Castro, A., 2013, Tonalite-granodiorite suites as cotectic systems: A review of experimental studies with applications to granitoid petrogenesis: Earth-Science Reviews, v. 124, p. 68–95, https://doi.org/10.1016/j.earscirev.2013.05.006.

Castro, A., 2020, The dual origin of I-type granites: The contribution from experiments, *in* Janoušek, V., et al., eds., Post-Archean Granitic Rocks: Petrogenetic Processes and Tectonic Environments: Geological Society of London Special Publication 491, p. 101–145, https://doi.org/10.1144/SP491-2018-110.

Castro, A., 2021, A non-basaltic experimental cotectic array for calc-alkaline batholiths: Lithos, v. 382–383, https://doi.org/10.1016/j.lithos.2020.105929.

Castro, A., and Stephens, W.E., 1992, Amphibole-rich polycrystalline clots in calc-alkaline granitic rocks and their enclaves: Canadian Mineralogist, v. 30, no. 4, p. 1093–1112.

Castro, A., Gerya, T., García-Casco, A., Fernández, C., Díaz Alvarado, J., Moreno-Ventas, I., and Loew, I., 2010, Melting relations of MORB-sediment mélanges in underplated mantle wedge plumes: Implications for the origin of cordilleran-type batholiths: Journal of Petrology, v. 51, no. 6, p. 1267–1295, https://doi.org/10.1093/petrology/egq019.

Castro, A., Moreno-Ventas, I., Fernández, C., Vujovich, G., Gallastegui, G., Heredia, N., Martino, R.D., Becchio, R., Corretgé, L.G., Díaz-Alvarado, J., García-Arias, M., and Liu, D.-Y., 2011, Petrology and SHRIMP U-Pb zircon geochronology of Cordilleran granitoids of the Bariloche area, Argentina: Journal of South American Earth Sciences, v. 32, p. 508–530, https://doi.org/10.1016/j.jsames.2011.03.011.

Castro, A., Vogt, K., and Gerya, T., 2013, Generation of new continental crust by sublithospheric silicic-magma relamination in arcs: A test of Taylor's andesite model: Gondwana Research, v. 23, no. 4, p. 1554–1566, https://doi.org/10.1016/j.gr.2012.07.004.

Claoue-Long, J.C., Compston, W., Roberts, J., and Fanning, C.M., 1995, Two Carboniferous ages: A comparison of SHRIMP zircon dating with conventional zircon ages and $^{40}Ar/^{39}Ar$ analysis, *in* Berggren, W.A., Kent, D.V., Aubry, M.-P., and Hardenbol, J., eds., Geochronology, Time Scales and Global Stratigraphic Correlation: Society for Sedimentary Geology (SEPM) Special Publication 54, p. 3–21.

Clift, P., and Vannucchi, P., 2004, Controls on tectonic accretion versus erosion in subduction zones: Implications for the origin and recycling of the continental crust: Reviews of Geophysics, v. 42, https://doi.org/10.1029/2003RG000127.

Cloos, M., and Shreve, R.L., 1988, Subduction-channel model of prism accretion, mélange formation, sediment subduction, and subduction erosion at convergent plate margins: 2. Implications and discussion: Pure and Applied Geophysics, v. 128, p. 501–545, https://doi.org/10.1007/BF00874549.

Codillo, E.A., Le Roux, V., and Marschall, H.R., 2018, Arc-like magmas generated by mélange-peridotite interaction in the mantle wedge: Nature Communications, v. 9, p. 2864, https://doi.org/10.1038/s41467-018-05313-2.

Cox, A., and Hart, R.B., 1986, Plate Tectonics. How it Works: Palo Alto, California, Blackwell, 418 p.

Cruden, A.R., McCaffrey, K.J.W., and Bunger, A.P., 2018, Geometric scaling of tabular igneous intrusions: Implications for emplacement and growth, *in* Breitkreuz, C., and Rocchi, S., eds., Physical Geology of Shallow Magmatic Systems: Dykes, Sills and Laccoliths: Cham, Switzerland, Springer International Publishing, p. 11–38, https://doi.org/10.1007/11157_2017_1000.

Cruz-Uribe, A.M., Marschall, H.R., Gaetani, G.A., and Le Roux, V., 2018, Generation of alkaline magmas in subduction zones by partial melting of mélange diapirs—An experimental study: Geology, v. 46, no. 4, p. 343–346, https://doi.org/10.1130/G39956.1.

Davidson, J.P., Harmon, R.S., Wörner, G., Harmon, R.S., and Rapela, C.W., 1991, The source of central Andean magmas; Some considerations, *in* Harmon, R.S., and Rapela, C.W., eds., Andean Magmatism and Its Tectonic Setting: Geological Society of America Special Paper 265, p. 233–244, https://doi.org/10.1130/SPE265-p233.

DeMets, C., Gordon, R.G., and Argus, D.F., 2010, Geologically current plate motions: Geophysical Journal International, v. 181, no. 1, p. 1–80, https://doi.org/10.1111/j.1365-246X.2009.04491.x.

DePaolo, D.J., 1981a, A neodymium and strontium isotopic study of the Mesozoic calc-alkaline granitic batholiths of the Sierra Nevada and Peninsular Ranges, California: Journal of Geophysical Research, v. 86, p. 10470–10488, https://doi.org/10.1029/JB086iB11p10470.

DePaolo, D.J., 1981b, Trace element and isotopic effects of combined wallrock assimilation and fractional crystallization: Earth and Planetary Science Letters, v. 53, no. 2, p. 189–202, https://doi.org/10.1016/0012-821X(81)90153-9.

Duhart, P., McDonough, M., Muñoz, J., Martin, M., and Villeneuve, M., 2001, El Complejo Metamórfico Bahía Mansa en la cordillera de la Costa del centro-sur de Chile (39°30′-42°00′S): Geocronología K-Ar, $^{40}Ar/^{39}Ar$ y U-Pb e implicancias en la evolución del margen sur-occidental de Gondwana: Revista Geológica de Chile, v. 28, p. 179–208, https://doi.org/10.4067/S0716-02082001000200003.

Echaurren, A., Oliveros, V., Folguera, A., Ibarra, F., Creixell, C., and Lucassen, F., 2017, Early Andean tectonomagmatic stages in north Patagonia: Insights from field and geochemical data: Journal of the Geological Society [London], v. 174, no. 3, p. 405–421, https://doi.org/10.1144/jgs2016-087.

Engebretson, D.C., Cox, A., and Gordon, R.G., 1985, Relative Motions Between Oceanic and Continental Plates in the Pacific Basin: Geological Society of America Special Paper 206, 59 p., https://doi.org/10.1130/SPE206-p1.

Fernández, C., and Castro, A., 2018, Mechanical and structural consequences of magma differentiation at ascent conduits: A possible origin for some mafic microgranular enclaves in granites: Lithos, v. 320–321, p. 49–61, https://doi.org/10.1016/j.lithos.2018.09.004.

Folguera, A., and Iannizzotto, N.F., 2004, The Lagos la Plata and Fontana fold-and-thrust belt: Long-lived orogenesis at the edge of western Patagonia: Journal of South American Earth Sciences, v. 16, no. 7, p. 541–566, https://doi.org/10.1016/j.jsames.2003.10.001.

Forsythe, R., 1982, The late Palaeozoic to early Mesozoic evolution of southern South America: A plate tectonic interpretation: Journal of the Geological Society [London], v. 139, no. 6, p. 671–682, https://doi.org/10.1144/gsjgs.139.6.0671.

Franke, D., 2013, Rifting, lithosphere breakup and volcanism: Comparison of magma-poor and volcanic rifted margins: Marine and Petroleum Geology, v. 43, p. 63–87, https://doi.org/10.1016/j.marpetgeo.2012.11.003.

Frost, B.R., Barnes, C.G., Collins, W.J., Arculus, R.J., Ellis, D.J., and Frost, C.D., 2001, A geochemical classification for granitic rocks: Journal of Petrology, v. 42, no. 11, p. 2033–2048, https://doi.org/10.1093/petrology/42.11.2033.

Gale, A., Dalton, C.A., Langmuir, C.H., Su, Y., and Schilling, J.-G., 2013, The mean composition of ocean ridge basalts: Geochemistry Geophysics Geosystems, v. 14, no. 3, p. 489–518, https://doi.org/10.1029/2012GC004334.

Gerya, T.V., and Meilick, F.I., 2011, Geodynamic regimes of subduction under an active margin: Effects of rheological weakening by fluids and melts: Journal of Metamorphic Geology, v. 29, no. 1, p. 7–31, https://doi.org/10.1111/j.1525-1314.2010.00904.x.

Gerya, T.V., and Yuen, D.A., 2003, Rayleigh-Taylor instabilities from hydration and melting propel 'cold plumes' at subduction zones: Earth and Planetary Science Letters, v. 212, no. 1–2, p. 47–62, https://doi.org/10.1016/S0012-821X(03)00265-6.

Gerya, T.V., Yuen, D.A., and Sevre, E.O.D., 2004, Dynamical causes for incipient magma chambers above slabs: Geology, v. 32, no. 1, p. 89–92, https://doi.org/10.1130/G20018.1.

Gordon, R.G., and Jurdy, D.M., 1986, Cenozoic global plate motions: Journal of Geophysical Research–Solid Earth, v. 91, no. B12, p. 12389–12406, https://doi.org/10.1029/JB091iB12p12389.

Grove, T., Parman, S., Bowring, S., Price, R., and Baker, M., 2002, The role of an H_2O-rich fluid component in the generation of primitive basaltic andesites and andesites from the Mt. Shasta region, N California: Contributions to Mineralogy and Petrology, v. 142, no. 4, p. 375–396, https://doi.org/10.1007/s004100100299.

Grove, T.L., Baker, M.B., Price, R.C., Parman, S.W., Elkins-Tanton, L.T., Chatterjee, N., and Müntener, O., 2005, Magnesian andesite and dacite lavas from Mt. Shasta, northern California: Products of fractional crystallization of H_2O-rich mantle melts: Contributions to Mineralogy and Petrology, v. 148, no. 5, p. 542–565, https://doi.org/10.1007/s00410-004-0619-6.

Gualda, G.A.R., Ghiorso, M.S., Lemons, R.V., and Carley, T.L., 2012, Rhyolite-MELTS: A modified calibration of MELTS optimized for silica-rich, fluid-bearing magmatic systems: Journal of Petrology, v. 53, p. 875–890, https://doi.org/10.1093/petrology/egr080.

Hammerli, J., Kemp, A.I.S., Shimura, T., Vervoort, J.D., EIMF, and Dunkley, D.J., 2018, Generation of I-type granitic rocks by melting of heterogeneous lower crust: Geology, v. 46, no. 10, p. 907–910, https://doi.org/10.1130/G45119.1.

Haschke, M., Günther, A., Melnick, D., Echtler, H., Reutter, K.-J., Scheuber, E., and Oncken, O., 2006a, Central and southern Andean tectonic evolution inferred from arc magmatism, *in* Oncken, O., Chong, G., Franz, G., Giese, P., Götze, H.-J., Ramos, V. A., Strecker, M.R., and Wigger, P., eds., The Andes: Active Subduction Orogeny: Berlin, Springer, p. 337–353, https://doi.org/10.1007/978-3-540-48684-8_16.

Haschke, M., Sobel, E.R., Blisniuk, P., Strecker, M.R., and Warkus, F., 2006b, Continental response to active ridge subduction: Geophysical Research Letters, v. 33, no. 15, L15315, https://doi.org/10.1029/2006GL025972.

Hervé, F., Pankhurst, R.J., Fanning, C.M., Calderón, M., and Yaxley, G.M., 2007, The South Patagonian batholith: 150 my of granite magmatism on a plate margin: Lithos, v. 97, no. 3, p. 373–394, https://doi.org/10.1016/j.lithos.2007.01.007.

Hervé, F., Calderón, M., and Faúndez, V., 2008, The metamorphic complexes of the Patagonian and Fuegian Andes: Geologica Acta, v. 6, p. 43–53.

Hildreth, W., and Moorbath, S., 1988, Crustal contributions to arc magmatism in the Andes of central Chile: Contributions to Mineralogy and Petrology, v. 98, p. 455–489, https://doi.org/10.1007/BF00372365.

Johannes, W., and Holtz, F., 1996, Petrogenesis and Experimental Petrology of Granitic Rocks: Berlin, Springer, 335 p.

Kelemen, P.B., 1995, Genesis of high-Mg# andesites and the continental crust: Contributions to Mineralogy and Petrology, v. 120, p. 1–19, https://doi.org/10.1007/BF00311004.

Kelemen, P.B., Hanghøj, K., and Greene, A., 2003, One view of the geochemistry of subduction-related magmatic arcs, with an emphasis on primitive andesite and lower crust, *in* Holland, H.D., Turekian, K.K., and Rudnick, R.L., eds., Treatise on Geochemistry, Volume 3: The Crust: Oxford, UK, Elsevier Pergamon, p. 593–659.

Kelley, K.A., Plank, T., Ludden, J., and Staudigel, H., 2003, Composition of altered oceanic crust at ODP Sites 801 and 1149: Geochemistry Geophysics Geosystems, v. 4, no. 6, 8910, https://doi.org/10.1029/2002GC000435.

Keppie, D.F., Currie, C.A., and Warren, C., 2009, Subduction erosion modes: Comparing finite element numerical models with the geological record: Earth and Planetary Science Letters, v. 287, p. 241–254, https://doi.org/10.1016/j.epsl.2009.08.009.

Kushiro, I., 1974, Melting of hydrous upper mantle and possible generation of andesitic magma: An approach from synthetic systems: Earth and Planetary Science Letters, v. 22, no. 4, p. 294–299, https://doi.org/10.1016/0012-821X(74)90138-1.
Larson, R.L., and Ladd, J.W., 1973, Evidence for the opening of the South Atlantic in the early cretaceous: Nature, v. 246, p. 209–212, https://doi.org/10.1038/246209a0.
Lee, C.T.A., Cheng, X., and Horodyskyj, U., 2006, The development and refinement of continental arcs by primary basaltic magmatism, garnet pyroxenite accumulation, basaltic recharge and delamination: Insights from the Sierra Nevada, California: Contributions to Mineralogy and Petrology, v. 151, no. 2, p. 222–242, https://doi.org/10.1007/s00410-005-0056-1.
Lonsdale, P., 2005, Creation of the Cocos and Nazca plates by fission of the Farallon plate: Tectonophysics, v. 404, p. 237–264, https://doi.org/10.1016/j.tecto.2005.05.011.
Ludwig, K.R., 2003, Isoplot 3.0: A Geochronological Toolkit for Microsoft Excel: Berkeley Geochronology Center Special Publication 4a, 71 p.
Marschall, H.R., and Schumacher, J.C., 2012, Arc magmas sourced from mélange diapirs in subduction zones: Nature Geoscience, v. 5, p. 862–867, https://doi.org/10.1038/ngeo1634.
Miyashiro, A., 1974, Volcanic rock series in island arcs and active continental margins: American Journal of Science, v. 274, no. 4, p. 321–355, https://doi.org/10.2475/ajs.274.4.321.
Molina, J.F., Moreno, J.A., Castro, A., Rodríguez, C., and Fershtater, G.B., 2015, Calcic amphibole thermobarometry in metamorphic and igneous rocks: New calibrations based on plagioclase/amphibole Al-Si partitioning and amphibole/liquid Mg partitioning: Lithos, v. 232, p. 286–305, https://doi.org/10.1016/j.lithos.2015.06.027.
Molina, J.F., Cambeses, A., Moreno, J.A., Morales, I., Montero, P., and Bea, F., 2020, A reassessment of the amphibole-plagioclase NaSi-CaAl exchange thermometer with applications to igneous and high-grade metamorphic rocks: American Mineralogist (in press), https://doi.org/10.2138/am-2021-7400.
Montero, P., and Bea, F., 1998, Accurate determination of $^{87}Sr/^{86}Sr$ and $^{143}Sm/^{144}Nd$ ratios by inductively coupled-plasma mass spectrometry in isotope geosciences: An alternative to isotope dilution analysis: Analytical Chemistry Acta, v. 358, p. 227–233.
Nakamura, N., 1974, Determination of REE, Ba, Fe, Mg, Na and K in carbonaceous and ordinary chondrites: Geochimica et Cosmochimica Acta, v. 38, p. 757–775, https://doi.org/10.1016/0016-7037(74)90149-5.
Nielsen, S.G., and Marschall, H.R., 2017, Geochemical evidence for mélange melting in global arcs: Science Advances, v. 3, https://doi.org/10.1126/sciadv.1602402.
Orts, D.L., Folguera, A., Encinas, A., Ramos, M., Tobal, J., and Ramos, V.A., 2012, Tectonic development of the North Patagonian Andes and their related Miocene foreland basin (41°30′–43°S): Tectonics, v. 31, TC3012, https://doi.org/10.1029/2011TC003084.
Pankhurst, R.J., Weaver, S.D., Herve, F., and Larrondo, P., 1999, Mesozoic–Cenozoic evolution of the North Patagonian batholith in Aysen, southern Chile: Journal of the Geological Society [London], v. 156, no. 4, p. 673–694, https://doi.org/10.1144/gsjgs.156.4.0673.
Pardo-Casas, F., and Molnar, P., 1987, Relative motion of the Nazca (Farallon) and South American plates since Late Cretaceous time: Tectonics, v. 6, no. 3, p. 233–248, https://doi.org/10.1029/TC006i003p00233.
Plank, T., and Langmuir, C.H., 1998, The chemical composition of subducted sediment and its consequences for the crust and mantle: Chemical Geology, v. 145, p. 325–394, https://doi.org/10.1016/S0009-2541(97)00150-2.
Qian, Q., and Hermann, J., 2013, Partial melting of lower crust at 10–15 kbar: Constraints on adakite and TTG formation: Contributions to Mineralogy and Petrology, v. 165, no. 6, p. 1195–1224, https://doi.org/10.1007/s00410-013-0854-9.
Reubi, O., and Blundy, J., 2009, A dearth of intermediate melts at subduction zone volcanoes and the petrogenesis of arc andesites: Nature, v. 461, p. 1269–1273, https://doi.org/10.1038/nature08510.
Ridolfi, F., and Renzulli, A., 2012, Calcic amphiboles in calc-alkaline and alkaline magmas: Thermobarometric and chemometric empirical equations valid up to 1,130°C and 2.2 GPa: Contributions to Mineralogy and Petrology, v. 163, no. 5, p. 877–895, https://doi.org/10.1007/s00410-011-0704-6.
Rodríguez, C., and Castro, A., 2017, Silicic magma differentiation in ascent conduits: Experimental constraints: Lithos, v. 272–273, p. 261–277, https://doi.org/10.1016/j.lithos.2016.12.017.
Rudnick, R.L., and Gao, S., 2003, Composition of the continental crust, *in* Rudnick, R.L., ed., The Crust, Volume 3: Oxford, Elsevier-Pergamon, p. 1–64.
Somoza, R., 1998, Updated Nazca (Farallon)–South America relative motions during the last 40 My: Implications for mountain building in the central Andean region: Journal of South American Earth Sciences, v. 11, no. 3, p. 211–215, https://doi.org/10.1016/S0895-9811(98)00012-1.
Somoza, R., and Ghidella, M.E., 2012, Late Cretaceous to recent plate motions in western South America revisited: Earth and Planetary Science Letters, v. 331–332, p. 152–163, https://doi.org/10.1016/j.epsl.2012.03.003.
Stern, C.R., 1991a, Comment on "Crustal contributions to arc magmatism in the Andes of central Chile" by W. Hildreth and S. Moorbath: Contributions to Mineralogy and Petrology, v. 108, no. 1, p. 241–246, https://doi.org/10.1007/BF00307341.
Stern, C.R., 1991b, Role of subduction erosion in the generation of Andean magmas: Geology, v. 19, no. 1, p. 78–81, https://doi.org/10.1130/0091-7613(1991)019<0078:ROSEIT>2.3.CO;2.
Stern, C.R., 2011, Subduction erosion: Rates, mechanisms, and its role in arc magmatism and the evolution of the continental crust and mantle: Gondwana Research, v. 20, p. 284–308, https://doi.org/10.1016/j.gr.2011.03.006.
Stern, C.R., 2020, The role of subduction erosion in the generation of Andean and other convergent plate boundary arc magmas, the continental crust and mantle: Gondwana Research, v. 88, p. 220–249, https://doi.org/10.1016/j.gr.2020.08.006.
Suárez, M., and De La Cruz, R., 2001, Jurassic to Miocene K-Ar dates from eastern central Patagonian Cordillera plutons, Chile (45°–48°S): Geological Magazine, v. 138, no. 1, p. 53–66, https://doi.org/10.1017/S0016756801004903.
Taylor, S.R., 1967, The origin and growth of continents: Tectonophysics, v. 4, no. 1, p. 17–34, https://doi.org/10.1016/0040-1951(67)90056-X.
Thompson, R.N., Morrison, M.A., Hendry, G.L., and Parry, S.J.P., 1984, An assessment of the relative roles of a crust and mantle in magma genesis: An elemental approach: Philosophical Transactions of the Royal Society of London, ser. A, v. 310, p. 549–590.
Thomson, S.N., and Hervé, F., 2002, New time constraints for the age of metamorphism at the ancestral Pacific Gondwana margin of southern Chile (42–52°S): Revista Geológica de Chile, v. 29, p. 255–271, https://doi.org/10.4067/S0716-02082002000200007.
Ulmer, P., Kaegi, R., and Müntener, O., 2018, Experimentally derived intermediate to silica-rich arc magmas by fractional and equilibrium crystallization at 1.0 GPa: An evaluation of phase relationships, compositions, liquid lines of descent and oxygen fugacity: Journal of Petrology, v. 59, no. 1, p. 11–58, https://doi.org/10.1093/petrology/egy017.
Vogt, K., Gerya, T.V., and Castro, A., 2012, Crustal growth at active continental margins: Numerical modeling: Physics of the Earth and Planetary Interiors, v. 192–193, p. 1–20, https://doi.org/10.1016/j.pepi.2011.12.003.
Vogt, K., Castro, A., and Gerya, T., 2013, Numerical modeling of geochemical variations caused by crustal relamination: Geochemistry Geophysics Geosystems, v. 14, no. 2, p. 470–487, https://doi.org/10.1002/ggge.20072.
von Huene, R., and Schöll, D.W., 1991, Observations concerning sediment subduction and subduction erosion, and the growth of continental crust at convergent ocean margins: Reviews of Geophysics, v. 29, p. 279–316, https://doi.org/10.1029/91RG00969.
Whitney, D.L., and Evans, B.W., 2010, Abbreviations for names of rock-forming minerals: The American Mineralogist, v. 95, p. 185–187, https://doi.org/10.2138/am.2010.3371.
Willner, A.P., Hervé, F., and Massonne, H.-J., 2000, Mineral chemistry and pressure-temperature evolution of two contrasting high-pressure–low-temperature belts in the Chonos Archipelago, southern Chile: Journal of Petrology, v. 41, no. 3, p. 309–330, https://doi.org/10.1093/petrology/41.3.309.
Wörner, G., Mamani, M., and Blum-Oeste, M., 2018, Magmatism in the Central Andes: Elements, v. 14, no. 4, p. 237–244, https://doi.org/10.2138/gselements.14.4.237.